# An Hourglass Circuit Motif Transforms a Motor Program via Subcellularly Localized Calcium Signaling in Muscle

**Steven R. Sando[1], Nikhil Bhatla[1,2,3], Eugene L. Q. Lee[1,3], H. Robert Horvitz[1,*]**

[1]Howard Hughes Medical Institute, Department of Biology, McGovern Institute for Brain Research, Massachusetts Institute of Technology, Cambridge, MA, 02139, USA

[2]Miller Institute, Helen Wills Neuroscience Institute, Department of Molecular and Cellular Biology, University of California, Berkeley, Berkeley, 94720, USA

[3]Department of Brain and Cognitive Sciences, Massachusetts Institute of Technology, Cambridge, MA, 02139, USA

*Correspondence: horvitz@mit.edu

Draft 5/30/2020

## Abstract

Neural control of muscle function is fundamental to animal behavior. In many cases, specific muscles can generate multiple distinct behaviors. Nonetheless, individual muscle cells are generally regarded as the smallest units of motor control. Here we report that muscle cells can alter their behavioral output by contracting subcellularly. We previously discovered that noxious tastes reverse the flow of material through the *C. elegans* pharynx, a neuromuscular pump, resulting in spitting. We now show that spitting is driven by the contraction of subcellular regions of individual muscle cells. Localized calcium signals accompany these contractions. Spitting is controlled by an "hourglass" circuit motif: parallel neural pathways converge onto a single motor neuron that differentially controls multiple muscles and the critical subcellular muscle compartment. In short, we find that subcellular muscle units enable modulatory motor control and propose that subcellular muscle contraction is a fundamental mechanism by which neurons can reshape motor function.

## Introduction

How animal nervous systems differentially control muscle function to generate the variety of flexible, context-appropriate behaviors necessary for survival and reproduction is a fundamental problem in neuroscience. In many cases, distinct behaviors must be performed using the same muscle or set of muscles. For example, the muscles of the human jaw and tongue control both feeding and speech, while the *Drosophila* wing muscles produce both flight and song (O'Sullivan *et al*., 2018). Neurons can elicit such different outcomes by altering the amplitudes and relative timing of muscle motions (Briggman and Kristan, 2008; Marder and Calabrese, 1996) or, in principle, by evoking entirely distinct modes of muscle function, with distinct spatial contraction parameters.

We are analyzing the neuromuscular control of behavior using the *C. elegans* feeding organ, the pharynx, as a model neuromuscular system. The pharynx (Figure 1A) is a neuromuscular pump that contracts rhythmically ("pumps") to generate the suction that ingests bacterial food (Avery and You, 2012). The pharynx contains 14 classes of neurons (20 neurons in total), 8 classes of muscles (20 muscles in total), 4 glands, and 16 structural cells, and the connectome of these cells has been completely described (Albertson and Thomson, 1976; Cook *et al*., 2019).

Behavioral functions are known for 9 of the 14 pharyngeal neuron classes (15 of the 20 total neurons). The two M2 neurons, single M4, and two MC neurons promote pumping and/or ingestion (Avery and Horvitz, 1987, 1989; Trojanowski *et al*., 2014); the two M3 and single I5 neurons regulate the timing of muscle relaxation (Avery, 1993); the

48 two I2 neurons inhibit pumping (Bhatla and Horvitz, 2015); the two I1 neurons promote
49 or inhibit pumping dependent on context (Dent *et al*., 2000; Trojanowski *et al*., 2014;
50 Bhatla *et al*., 2015); the two NSM neurons regulate locomotion and feeding in response
51 to food or food-related odors (Sawin *et al*., 2000; Li *et al*., 2012; Flavell *et al*., 2013;
52 Rhoades *et al*., 2019); and, as described in more detail below, the single M1 neuron
53 controls spitting behavior (Bhatla *et al*., 2015).

54 We previously found that short-wavelength violet or ultraviolet (UV) light inhibits
55 *C. elegans* feeding behavior and that this modulation likely is mediated by light-
56 generated reactive oxygen species (ROS) and thus reflects a response to noxious taste
57 stimuli (Bhatla and Horvitz, 2015). Consistent with this hypothesis, the same genes and
58 neurons required for light-induced feeding inhibition are also required for the inhibition of
59 feeding by the ROS hydrogen peroxide ($H_2O_2$) (Bhatla and Horvitz, 2015). Because we
60 and others have found that light and ROS act similarly to elicit behavioral responses
61 (Hill and Schaefer, 2009; Kim *et al*., 2013b; Kim and Johnson, 2014; Guntur *et al*., 2015;
62 Du *et al*., 2016; Arenas *et al*., 2017; Birkholz and Beane, 2017; Guntur *et al*., 2017), and
63 because of the high precision with which light can be controlled as an experimental
64 stimulus, we are using light as a tool to analyze how the neuromusculature of the
65 pharynx produces behavioral responses to noxious taste stimuli such as $H_2O_2$.

66 We found that upon exposure to short-wavelength light, pharyngeal pumping
67 rapidly stops ("acute inhibition") and then transiently resumes ("burst pumping"; Figure
68 1B). After the removal of light, the pumping rate is depressed and slowly recovers

69 (“recovery”) to the 4-5 Hz of normal feeding over about a minute (Bhatla and Horvitz,
70 2015). Our previous studies implicated four classes of pharyngeal neurons in the
71 pumping response to light (Bhatla and Horvitz, 2015; Bhatla *et al*., 2015). Light inhibits
72 pumping by altering the activity of the I1, I2, and MC neurons. Subsequently, the M1
73 motor neuron promotes the burst pumping phase, during which the flow of material
74 through the anterior pharynx is reversed, producing a spitting behavior that ejects
75 ingested material from the pharynx.

76 We now report that light transforms feeding pumps into spitting pumps -- i.e.
77 reverses the direction in which material is driven by pharyngeal pumping -- by inducing
78 sustained contractions of subcellular regions of individual muscle cells, the three pm3
79 pharyngeal muscle cells. Spatially restricted calcium signals are localized to the regions
80 of pharyngeal muscle undergoing contraction and are controlled by the M1 neuron. M1
81 sits at the waist of an “hourglass” circuit motif, in which multiple upstream sensory
82 neurons converge on M1, which in turn makes divergent outputs onto multiple muscle
83 classes that control distinct subcomponents of the spitting reflex. Weak activation of M1
84 via a subset of upstream neurons can evoke a subset of M1’s motor outputs, producing
85 an attenuated variant of spitting and showing how graded neuronal activation can
86 produce context-appropriate variations of a core behavior. Together, our results provide
87 an example of how muscle function can be modulated at a subcellular level to produce
88 flexible, contextual behavior and identifies subcellularly localized calcium as a
89 mechanistic basis of such modulation.

## Results

### Worms Spit as a Consequence of the Sustained Contraction of Anterior Pharyngeal Muscles

We previously defined burst pumping as the transient increase in pumping rate that follows acute light-induced pumping inhibition (Figure 1B) (Bhatla and Horvitz, 2015). Because 365 nm (UV) light evokes burst pumping most robustly (Bhatla and Horvitz, 2015), we used this wavelength in the experiments described below. We further characterized the burst pumping phase and observed that there are three alterations to pharyngeal function that occur during burst pumping: (a) pumping rate increases; (b) a valve that closes to capture food during feeding instead remains open, causing pharyngeal pumps to conclude in the spitting of pharyngeal contents; and (c) a filter that otherwise restricts particle influx opens, facilitating the rinsing of the pharyngeal lumen.

In this work, we first confirmed that pumping rate increases during burst pumping, as reported previously (Bhatla and Horvitz, 2015). We scored pumping in the burst pumping phase in real time by eye, using the assay validated by Bhatla and Horvitz (2015) and based on the rate of contraction of the grinder ("grinder pumps"), a readily-observed cuticular structure in the terminal bulb (Figure 1A and 1B).

We next confirmed and extended the previous observation that worms spit during the burst pumping phase (Bhatla *et al*., 2015). We distinguished feeding and spitting pumps by recording high-speed videos of worms feeding on a mixture of *E. coli*

110 bacterial food and comparably-sized 1 μm polystyrene beads (Fang-Yen *et al*., 2009;
111 Bhatla *et al*., 2015). We designated pumps that trapped ingested material in the anterior
112 pharynx as feeding pumps (Video 1) and pumps that failed to trap material as spitting
113 pumps (Video 2; Figure 1C). We previously found that violet light (436 nm) induces
114 spitting (Bhatla *et al*., 2015) and replicated this result using UV light (365 nm) (Figure
115 1C-1E). Consistent with the hypothesis that the response to light reflects a response to
116 light-generated ROS, the odor of $H_2O_2$ also induced spitting (Figure 1—figure
117 supplement 1A).

118 We then identified the biomechanical mechanism by which particle flow is
119 reversed to produce spitting. In feeding, contraction of the pharyngeal muscles opens
120 the lumen of the pharynx, generating suction and drawing food and fluid inwards. Two
121 cuticular structures project from pharyngeal muscle into the lumen of the anterior
122 pharynx and buccal cavity: the metastomal flaps and the pharyngeal valve (Figure 1A)
123 (Albertson and Thomson, 1976). The metastomal flaps were previously shown to limit
124 the size and flow of particles that enter the pharyngeal lumen from the buccal cavity
125 (Fang-Yen *et al*., 2009). For this reason, we will refer to the metastomal flaps as the
126 "metastomal filter." The pharyngeal valve is located immediately posterior to the filter
127 and prevents the escape of ingested particles from the pharyngeal lumen to the buccal
128 cavity: prior to the onset of pharyngeal muscle relaxation, the pharyngeal valve closes,
129 sealing the anterior end of the lumen to retain bacteria while fluid is released via
130 channels that border the lumen (Fang-Yen *et al*., 2009). Given the importance of the

131 pharyngeal valve in feeding, we hypothesized that spitting involves a modulation of the
132 motions of this structure. We recorded videos of animals feeding and spitting under a
133 coverslip such that the anterior pharyngeal muscles and lumen were clearly visualized.
134 As reported previously (Fang-Yen *et al*., 2009), feeding pumps involved the closure of
135 the pharyngeal valve, thus trapping food (Figure 1F; Video 3). By contrast, spitting
136 pumps were characterized by a strikingly different motion: rather than relaxing and
137 closing at each pump's conclusion, the anterior tip of the pharynx remained contracted -
138 - i.e., open -- throughout the pumping cycle (Figure 1F; Video 4). This sustained
139 contraction prevented the pharyngeal valve from closing and capturing food at the end
140 of the pump, such that closure of the lumen expelled the pharyngeal contents. These
141 open-valve pumping motions occurred specifically during the burst pumping phase,
142 confirming that they are specific to spitting (Figure 1—figure supplement 1B and 1C).

143 Finally, a third aspect of pharyngeal behavior was altered by light in the burst
144 pumping phase. As reported previously (Fang-Yen *et al*., 2009), the metastomal filter
145 was typically partially closed during feeding, such that material accumulated in the
146 buccal cavity and filtered only gradually into the pharynx (Figure 1C and 1G; Video 1).
147 We observed that during spitting, however, material moved freely from the buccal cavity
148 into the pharynx (Video 2), indicating that the metastomal filter opened during spitting
149 (Figure 1C, 1G). Thus, in combination with the opening of the pharyngeal valve, this
150 opening of the metastomal filter produced a rinsing effect, in which large amounts of
151 material were drawn into and then expelled from the pharynx.

152 Although the metastomal filter was typically partially closed during feeding, we
153 noticed that the filter was open during an average of up to 25% of feeding pumps
154 (Figure 1G, Video 5). Because opening the filter significantly increased the amount of
155 material ingested during these pumps, we designated such pumps as “gulps”.

156 In summary, we found that the spitting reflex is characterized by three changes to
157 pharyngeal behavior: (a) the pumping rate increases; (b) the pharyngeal valve remains
158 open instead of closing, producing spitting; and (c) the metastomal filter opens,
159 increasing the volume of material rinsed in and out with each pump. These changes
160 transform the pharyngeal motor program from one that promotes feeding into one that
161 promotes spitting from and rinsing of the procorpus (Figure 1A and 1H).

162

163 **Subcellularly Localized Muscle Contractions and Calcium Increases Open the**
164 **Pharyngeal Valve to Produce Spitting**

165 We next asked which muscles control the light-induced spitting reflex. The anterior
166 pharynx contains three pharyngeal muscle classes: pm1, pm2, and pm3 (Figure 2A).
167 pm1 is a single hexanucleate cell, while the pm2 and pm3 classes consist of three
168 binucleate cells each. The pm1 and pm2 muscles, small cells of unknown function, form
169 a ring around the anterior opening of the pharynx. The metastomal filter protrudes from
170 this ring into the buccal cavity (Figure 2A) such that contraction of the radially arranged
171 myofilaments of the pm1 and/or pm2 muscles would be expected to pull the filter open

172 and thus expand the aperture of the anterior pharynx. The pm3 muscles make up the
173 remainder of the musculature of the procorpus, and the pharyngeal valve protrudes
174 from their anterior ends. Because the filter and valve are held open in spitting, we
175 hypothesized that spitting involves the sustained contraction of some or all of pm1, pm2,
176 and/or the anterior end of pm3.

177 We sought to determine the roles of these muscles in spitting. Because ablation
178 of the pm3s results in lethality (Leon Avery, personal communication, March 2020), we
179 laser-killed the pm1 and pm2 muscles singly and in combination to determine what, if
180 any, function they have in spitting. Laser ablation of pm1, the pm2s, or both classes
181 together did not eliminate burst pumping or spitting (Figure 2B-2E), indicating that,
182 unexpectedly, the pm3s can suffice to open the pharyngeal valve and produce spitting.
183 In other words, the contraction of a subcellular region of the pm3 muscles must be
184 sufficient to open the valve. Specifically, the anterior regions of the pm3s underwent
185 sustained contraction while the rest of the muscles rhythmically contracted and relaxed
186 in animals in which the pm1 and pm2 muscles were ablated.

187 We were surprised to see the uncoupling of apparently separable subdomains --
188 the anterior end and the rest of the muscle cell -- within each of the pm3 muscle cells.
189 We then examined the physiological mechanism that produces these sustained and
190 spatially restricted muscle contractions in the pm3s. Given the central role of
191 intracellular calcium in initiating muscle contraction (Kuo and Ehrlich, 2015), we
192 expressed the calcium reporter GCaMP3 (Tian *et al*., 2009) in pharyngeal muscle and

193 imaged calcium changes in the pharynxes of immobilized animals (Kim *et al*., 2013a).
194 Immobilization inhibits pumping, and light stimulated pumping by immobilized animals
195 just as it does to produce burst pumping by free-moving animals. Light-stimulated
196 pumps were both dependent on the M1 neuron, which we previously showed to be
197 necessary for spitting (Bhatla *et al*., 2015), and resulted in the expulsion of previously
198 ingested mineral oil, as is the case for spitting by free-moving animals (Figure 2—figure
199 supplement 1A and data not shown).

200 When we stimulated pumps with light, we detected calcium increases across the
201 procorpus and the anterior and terminal bulbs, indicating that functional GCaMP was
202 present in these regions (Video 6, Figure 2F-2H). Interestingly, while calcium in most
203 pharyngeal regions rose and fell over the course of a pump, we observed sustained
204 calcium signals at the tip of the pharynx; these signals persisted continuously
205 throughout the pump cycle (Figure 2G). Additionally, during some trials this anterior
206 region responded with a sustained rise in calcium even when the rest of the pharynx did
207 not respond (Figure 2I). Consistent with previous reports (Kerr *et al*., 2000; Shimozono
208 *et al*., 2004), we did not observe spatially restricted calcium signals in the anterior
209 pharynx during feeding pumps stimulated with serotonin, indicating that these localized
210 calcium transients are specific to spitting (data not shown). The location and temporal
211 dynamics of the sustained calcium signals coincided precisely with the sustained
212 muscle contractions that we observed during spitting behavior, strongly suggesting that
213 they are part of the physiological mechanism driving subcellular contraction.

While the pm1 and pm2 muscles were not necessary for spitting, their ablation altered other aspects of pharyngeal function. First, pm2-ablated animals were partially defective in opening the metastomal filter, such that the filter was often closed during spitting (Video 7, Figure 2J). Second, consistent with a previous observation (L. Avery and C. Fang-Yen, personal communication, March 2020), ablation of pm1 eliminated the metastomal filter (Figure 2—figure supplement 1B and 1C; data not shown). For this reason, we were unable to determine whether pm1 is also involved in opening the filter. However, because pm2-ablated animals were not completely defective in opening the filter (Figure 2J) and pm1 is the only other muscle positioned to perform this function, we think it likely that pm1 contributes to the opening of the filter as well.

Taken together, and consistent with the anatomy of the anterior pharynx, our results indicate that the pm1, pm2, and pm3 muscles play specialized roles in controlling pharyngeal particle flow: the pm2 and likely the pm1 muscles actively open the metastomal filter, increasing the aperture size of the anterior lumen and thus facilitating particle influx, while a subcellular anterior compartment of the pm3s opens the pharyngeal valve via subcellular calcium signaling, thus producing spitting.

**Pharyngeally-Expressed Gustatory Receptor Orthologs *lite-1* and *gur-3* Play Major and Minor Roles, Respectively, in the Light-Induced Spitting Reflex**

233 Previously described *C. elegans* locomotory and pharyngeal responses to light depend
234 on the gustatory receptor orthologs *lite-1* and/or *gur-3*, which are expressed in a number
235 of pharyngeal and extra-pharyngeal neurons (Edwards *et al*., 2008; Liu *et al*., 2010;
236 Bhatla and Horvitz, 2015). We asked if gustatory receptor orthologs similarly control the
237 light-induced spitting reflex. Burst pumping rate was wild-type in animals carrying null
238 alleles of *gur-3* (Bhatla and Horvitz, 2015) or its paralogs *egl-47/gur-1, gur-4,* and *gur-5*
239 (Figure 3A and Figure 3—figure supplement 1A-1D). *lite-1* null mutants (Edwards *et al*.,
240 2008) could not be tested directly, because they exhibit significant defects in light-
241 induced pumping inhibition (Bhatla and Horvitz, 2015) (Figure 3B and 3C).

242 To examine the role of *lite-1* in burst pumping, we tested *lite-1* mutants in an *eat-*
243 *2* mutant background. *eat-2* mutants are severely defective in feeding pumping (Raizen
244 *et al*., 1995) but not in burst pumping (Figure 3D). Thus, the burst pumping rate rises
245 above the slow *eat-2* feeding pumping rate and can be scored even in animals defective
246 in light-induced inhibition of feeding. We found that *lite-1* but not *gur-3* was required for
247 burst pumping in the *eat-2* background, a defect that was rescued by a wild-type copy of
248 *lite-1* (Figure 3D-3G). Thus, light-induced stimulation of pumping requires *lite-1* but not
249 *gur-3.*

250 These experiments established a role for *lite-1* in controlling burst pumping. To
251 determine directly whether *lite-1* and/or *gur-3* are required for spitting -- i.e., the opening
252 of the pharyngeal valve -- we assayed light-induced spitting in *lite-1* and *gur-3* single
253 mutants and *lite-1 gur-3* double mutants. Both *gur-3* and *lite-1* mutants exhibited less

254 spitting than controls, and *lite-1* mutants also displayed a dramatic reduction in peak
255 spiting rate compared to wild-type animals (Figure 3H-3J and 3N). More strikingly, *lite-1*
256 *gur-3* double mutants did not spit in response to light (Figure 3K). Rescue transgenes
257 expressing wild-type copies of either *lite-1* (Bhatla and Horvitz, 2015) or *gur-3* (this
258 study) restored light-induced spitting in *lite-1 gur-3* double mutants (Figure 3L-3N). *lite-1*
259 mutants were additionally defective in opening the metastomal filter (Figure 3O).
260 Although *gur-3* mutants also displayed qualitatively reduced opening of the filter, this
261 reduction was not statistically significant (Figure 3O). Together, these results indicate
262 that both *lite-1* and *gur-3* function in light-induced spitting and opening of the filter, with
263 *lite-1* likely playing a greater role.

264 Next we assayed the pharyngeal muscle calcium response to light in *lite-1* and
265 *gur-3* mutants. *gur-3* mutants resembled wild-type animals (Figure 3P), while *lite-1*
266 mutants were almost completely defective in the pharyngeal muscle calcium response
267 to light, except for a very weak, fast response (Figure 3Q). This fast response depended
268 on *gur-3*, as the response of *lite-1 gur-3* double mutants was completely defective
269 (Figure 3R). Thus, consistent with our behavioral observations, *lite-1* and *gur-3* function
270 redundantly in light-induced calcium increases in pharyngeal muscle, with *lite-1* playing
271 a major role and *gur-3* playing a minor role.

272 Taken together, these results indicate that *lite-1* and *gur-3* both contribute to
273 light-induced spitting. *lite-1* is necessary for the full response -- i.e., a robust increase in
274 pharyngeal muscle calcium, pumping rate increase, and opening of the pharyngeal

275 valve and metastomal filter -- while *gur-3* is sufficient in the absence of *lite-1* to produce
276 an attenuated response (weak activation of pharyngeal muscle, partial opening of the
277 valve, and opening of the filter).

278

279 **The M1 Pharyngeal Neuron Innervates the Pharyngeal Valve and Controls Light-**
280 **Induced Spitting**

281 The M1 pharyngeal neuron is the only major source of innervation of the pm1, pm2, and
282 pm3 muscles at the anterior tip of the pharynx (Albertson and Thomson, 1976), in the
283 same region as the metastomal filter, the pharyngeal valve, and the subcellular muscle
284 contractions we observed during spitting (Figure 4A), suggesting that M1 is the motor
285 neuron that controls spitting. We previously found that M1 is required for spitting
286 induced by violet light (Bhatla *et al*., 2015). We first confirmed that M1 is also required
287 for spitting induced by UV light, which, as noted above, we used throughout this study to
288 induce spitting. We laser-killed M1 and also generated an M1 genetic-ablation strain in
289 which the mammalian caspase ICE (Cerretti *et al*., 1992; Thornberry *et al*., 1992; Zheng
290 *et al*., 1999) is expressed under an M1-specific promoter. Both laser and genetic
291 ablation of M1 eliminated UV light-induced burst pumping and spitting (Figure 4B-4E
292 and Figure 4—figure supplement 1A-C), and genetic ablation of M1 eliminated burst
293 pumping in *eat-2* mutants (Figure 4—figure supplement 1D). Laser ablation of M1 also
294 eliminated the spatially restricted calcium signals in anterior pharyngeal muscles (Figure

295 4F), consistent with their being induced by M1. We could not directly determine whether
296 ablation of M1 altered the function of the metastomal filter, because M1-ablated animals
297 did not spit and rarely pumped in the presence of light (but see below). We conclude
298 that the M1 neuron is required for UV light-induced burst pumping, spitting, and muscle
299 calcium physiology.

300 We observed that the pumping rate of M1-ablated animals recovered significantly
301 more quickly than did controls after stimulation with light and that these pumps, in
302 contrast to typical pumps in which the procorpus and grinder contract together, were
303 characterized by contractions of the grinder but not the procorpus (Figure 4—figure
304 supplement 1E-1H). These observations suggest that in addition to controlling pumping
305 and spitting in the burst pumping phase, M1 also inhibits the grinder during the recovery
306 phase.

307 Given that light-induced spitting requires M1, we asked whether M1 is acutely
308 activated by light. We generated transgenic animals expressing the calcium reporter
309 GCaMP6s (Chen *et al*., 2013) in M1 and measured light-induced calcium changes. As
310 indicated by robust GCaMP6s fluorescence increases, light increased M1 somatic
311 calcium levels, consistent with an acute function for M1 in spitting (Figure 4G-4I, Video
312 8).

313 We next asked if *lite-1* and *gur-3* control M1's calcium response to light. *lite-1* is
314 expressed in M1 (Bhatla and Horvitz, 2015; Taylor *et al*., 2019). The *gur-3* expression
315 pattern was first determined using extrachromosomal arrays expressing GFP under the

316 *gur-3* promoter (Bhatla and Horvitz, 2015) and subsequently examined using single-cell
317 transcriptomic analysis of the *C. elegans* nervous system (Taylor *et al*., 2019). Although
318 neither method detected *gur-3* expression in M1, when we integrated the previously-
319 generated extrachromosomal arrays into the genome we noted that, in addition to being
320 expressed in the I2 and I4 neurons as reported previously (Bhatla and Horvitz, 2015),
321 the stably integrated *gur-3*$_{promoter}$*::GFP* transgene was also expressed in M1 and
322 another pharyngeal neuron, MI (Figure 3—figure supplement 1E and 1F), consistent
323 with a function for both *lite-1* and *gur-3* in M1. As was the case with pharyngeal muscle
324 calcium increases, *lite-1* and *gur-3* were required for light-induced calcium increases in
325 the M1 soma (Figure 4J-4L, with *lite-1* and *gur-3* respectively playing major and minor
326 roles, indicating that the differential requirement for *lite-1* and *gur-3* in spitting occurs at
327 or upstream of M1's activation.

328 We then asked if M1 might be activated directly by light, as suggested by its
329 expression of *lite-1* and *gur-3*, or whether it instead is activated indirectly by input from
330 other light-sensitive neurons via synaptic, humoral (i.e., dense core vesicle), or gap
331 junction inputs. Synaptic and humoral dense-core vesicle signaling respectively require
332 *unc-13*, which encodes the *C. elegans* homolog of UNC13A (Maruyama and Brenner,
333 1991; Richmond *et al.*, 1999, 2001), and *unc-31,* which encodes the *C. elegans*
334 homolog of CADPS/CAPS (Berwin *et al*., 1998), so we examined light-induced M1
335 calcium responses in these mutants. In both *unc-13(s69)* reduction-of-function mutants
336 (Richmond *et al*., 1999) -- null mutations are lethal (Kohn *et al*., 2000) -- and *unc-*

337 *31(u280)* presumptive null mutants (Speese *et al*., 2007), M1's calcium response was
338 reduced in magnitude but still significant (Figure 4M-4P). These results indicate that M1
339 likely can function as a cellular photoreceptor but do not preclude the possibility that
340 M1's activation occurs through residual *unc-13* function, gap junctions, or a pathway in
341 which *unc-13* and *unc-31* function redundantly.

342 To determine whether acute activation of M1 is sufficient to produce spitting, we
343 expressed channelrhodopsin 2 (ChR2) (Nagel *et al*., 2003; Boyden *et al*., 2005) in M1.
344 Because the light used to activate ChR2 also activates the endogenous pharyngeal
345 response to light, we performed these experiments on *lite-1 gur-3* mutant animals.
346 While no *lite-1 gur-3* mutant animals grown in the absence of the essential ChR2
347 cofactor all-*trans* retinal (ATR) showed spitting behavior in response to stimulation with
348 470 nm blue light, 25% of animals grown with ATR did so when illuminated (Figure 4Q
349 and 4R). Thus, optogenetic activation of M1 can produce spitting behavior, although not
350 as efficiently as UV light does in the wild-type background.

351 Next, we asked what neurotransmitter or neurotransmitters M1 uses to activate
352 pharyngeal muscle. M1 expresses the cholinergic markers *unc-17* and *cha-1* (Franks *et*
353 *al*., 2009; Taylor *et al*., 2019), and consistent with a cholinergic function for M1 we found
354 that animals with loss-of-function mutations in genes required for signaling by
355 acetylcholine (ACh) but not by other neurotransmitters were severely defective in burst
356 pumping, as were *ric-1* mutants, which are defective in nicotinic ACh receptor
357 maturation (Halevi *et al*., 2002) (Figure 4—figure supplement 1I-1R).

358 We assayed the burst pumping behavior of 36 strains, each carrying mutations in
359 one of 36 of the 37 known *C. elegans* ACh receptors (null mutation in the 37th receptor,
360 *acr-9*, results in lethality) (The *C. elegans* Deletion Mutant Consortium, 2012). While
361 several strains showed modest defects, none was strikingly defective, suggesting that
362 multiple acetylcholine receptors function redundantly downstream of M1 (Figure 4—
363 figure supplement 2A-2P').

364 Together these observations confirmed and extended our previous finding that
365 M1 is necessary for spitting, additionally showing that it controls spatially-restricted
366 muscle calcium signals, that it is acutely activated by light, and that its activation can
367 suffice for spitting.

368

369 **The *gur-3*-Expressing I2 and I4 Neurons Can Weakly Activate M1 to Open the**
370 **Metastomal Filter and Pharyngeal Valve Without Increasing Pumping Rate**

371 The M1 neuron's expression of *lite-1* and *gur-3* suggests that M1 is a likely site of action
372 of *lite-1* and *gur-3* in the spitting response to light. However, *unc-13* and *unc-31* mutants
373 were significantly reduced in M1 activation (Figure 4M-4P), consistent with the
374 possibility that other *lite-1* and/or *gur-3* neurons provide stimulatory inputs to M1.

375 To identify additional light-sensing neurons upstream of M1, we first focused on
376 pharyngeal neurons known to express *gur-3*. The pharyngeal I2 neurons express *gur-3*
377 and control light-induced pumping inhibition (Bhatla and Horvitz, 2015). Since the I2s

378 form electrical and chemical synapses with the M1 neuron (Albertson and Thomson,
379 1976), we tested the hypothesis that they provide functional inputs to M1 for the
380 induction of spitting by expressing a wild-type copy of *gur-3* under an I2-specific
381 promoter (Bhatla and Horvitz, 2015) in *lite-1 gur-3* double mutants. I2-specific rescue of
382 *gur-3* restored robust light-induced spitting, opening of the metastomal filter, and weak
383 M1 calcium increases to *lite-1 gur-3* double mutants, indicating that light can activate
384 M1 via *gur-3* function in the I2 neurons (Figure 5A-D). Laser ablation of M1 suppressed
385 this *gur-3*-dependent spitting and opening of the metastomal filter (Figure 5E-5G),
386 showing that the I2 neurons act via (or possibly in parallel to) M1 to induce spits and
387 open the filter.

388 Since the I2 neurons can strongly stimulate spitting, we next asked if they could
389 increase pumping rates in slow-pumping *eat-2* mutants. Light did not increase the
390 pumping rate of *eat-2*; *lite-1 gur-3;* $I2_{promoter}$*::gur-3(+)* animals (Figure 5H). Thus, while
391 the I2 neurons can activate M1 and thereby open the pharyngeal valve and metastomal
392 filter, they are unable to activate M1 sufficiently strongly to drive pumping rate
393 increases. This finding is consistent with our calcium imaging results indicating the I2
394 neurons can activate M1 only weakly (Figure 5D) and with our observation that *lite-1,*
395 but not *gur-3,* is required for burst pumping (Figure 3D-3G).

396 Because prior work showed that the I2s inhibit pumping in response to light
397 (Bhatla and Horvitz, 2015), we were initially surprised to see that *lite-1 gur-3*;
398 $I2_{promoter}$*::gur-3(+)* animals inhibited pumping only weakly (Figure 5E). Interestingly, after

399 we ablated M1 in these animals, we observed robust light-induced pumping inhibition
400 (Figure 5E, 5F, and 5I). This finding suggests that the I2 neurons' stimulatory effect on
401 M1 outweighs their inhibitory effect on pharyngeal muscle. Initially, it seemed
402 paradoxical that the I2s would function in this manner. However, when we compared the
403 rate of feeding pumps (i.e., pumps that capture food) in M1- and mock-ablated *lite-1*
404 *gur-3;* $I2_{promoter}$*::gur-3* animals, it became clear that the I2s' activation of M1 actually
405 serves to reduce the overall feeding rate, because activating M1 eliminates feeding
406 pumps by turning them into spits (Figure 5J). Thus, rather than simply acting as
407 nonspecific inhibitors of the rates of both feeding and spitting pumps, the I2s specifically
408 function to reduce food intake via two mechanisms: direct inhibition of feeding by
409 hyperpolarizing pharyngeal muscles (Bhatla and Horvitz, 2015; Bhatla *et al*., 2015) and
410 indirect conversion of feeding pumps into spits by activating M1 (Figure 5K).

411 We used an I2-specific genetic-ablation transgene (Bhatla and Horvitz, 2015) to
412 kill the I2 neurons in wild-type and *lite-1* genetic backgrounds. Spitting persisted after
413 ablation of the I2 neurons in both cases (Figure 5L and 5M), confirming that the I2
414 neurons are not necessary for spitting. Thus, *gur-3*-expressing neurons other than the
415 I2 neurons can promote spitting.

416 *gur-3* is also expressed in the pharyngeal I4 neuron (Figure 6A), which is of
417 unknown function. I4 is activated by light (Bhatla and Horvitz, 2015) and synapses onto
418 M1 (Albertson and Thomson, 1976). To determine if I4 contributes to M1's *gur-3*-
419 dependent activation by light, we laser-killed the I2s and I4 of *lite-1* mutants singly and

420 in combination and assayed spitting behavior. While *lite-1* animals in which either the
421 I2s or I4 were ablated alone exhibited spitting behavior in response to light, I4 ablation
422 significantly reduced the spitting of *lite-1* I2-ablated animals such that I2/I4 double-
423 ablated animals exhibited significantly delayed spitting (Figure 6B-6F), suggesting that
424 the I2 and I4 neurons are required redundantly for rapid light-induced spitting.
425 Consistent with the I2s and I4 acting together to promote activation of M1, we detected
426 small light-induced M1 calcium increases in mock-*,* I2-, and I4-ablated *lite-1* animals but
427 not in I2/I4 double-ablated *lite-1* animals (Figure 6G). I2-, I4-, and I2/I4-ablated animals
428 seemed to open the metastomal filter slightly less often than did mock-ablated controls,
429 but this small difference was not statistically significant (Figure 6H). We noticed that *lite-*
430 *1*; I4-ablated animals (Figure 6D) appeared to inhibit pumping more strongly than did
431 *lite-1;* mock-ablated animals (Figure 6B) and that this inhibition depended on the I2s
432 (Figure 6C). Thus, it is possible that I4 regulates the I2s' inhibition of pumping. Similarly,
433 the inhibition of *lite-1* I4-ablated animals (Figure 6D) was also much stronger than that
434 of *lite-1 gur-3;* $I2_{promoter}$*::gur-3(+)* animals (Figure 5B and 5E)*,* suggesting that *gur-3*
435 functions in neurons other than the I2s and I4 to regulate the balance between
436 excitation and inhibition of pumping. Finally, these results are also consistent with *gur-*
437 *3'*s functioning in another upstream neuron that acts via I4, rather than in I4 itself. In
438 short, our ablation data suggest but do not prove that I4 can promote spitting.

439 To verify that the spitting we observed in these experiments was M1-dependent,
440 we killed M1 in combination with the I2 and I4 neurons of *lite-1* mutants. As expected,

441 ablation of M1 eliminated spitting in all conditions (Figure 6I-6M). Consistent with our
442 observation that I2 inhibits pumping in M1-ablated animals (Figure 5F), we found that
443 M1-, and M1/I4-ablated animals inhibited pumping in response to light and that triple-
444 ablated animals lacking M1, I2, and I4 were defective in pumping inhibition (Figure 66J,
445 6L-6N). Some M1/I2-ablated animals inhibited pumping in response to light, suggesting
446 that the I4 neuron might inhibit pumping in a manner similar to the I2 neurons, but this
447 effect was not statistically significant (Figure 6K and 6N).

448 Because ablating the I2 and I4 neurons together failed to completely eliminate
449 spitting, *gur-3* likely functions in one or more additional neurons. In addition to being
450 expressed in M1 and MI, *gur-3* is also expressed in the extra-pharyngeal AVD neurons.
451 Thus, these cells or others might be additional sites of residual *gur-3* function. In short,
452 at least the I2 and I4 neurons are required redundantly to inhibit pumping and promote
453 *gur-3*- and M1-dependent spitting.

454

455 **Discussion**

456 To understand how the nervous system adapts the output of a single set of muscles to a
457 changing environment, we analyzed the spitting reflex of the *C. elegans* pharynx. This
458 reflex comprises three parallel behavioral components: an increase in pumping rate, the
459 opening of the pharyngeal valve, and the opening of the metastomal filter. Opening the
460 pharyngeal valve permits the expulsion of ingested material, while opening the
461 metastomal filter allows the worm to flush in and out large amounts of fluid and particles

462 not previously in the pharynx, apparently rinsing its mouth in response to a bad taste
463 (Figure 7A). The pm2 and likely the pm1 pharyngeal muscles open the metastomal
464 filter, while a subcellular compartment of the pm3 muscles opens the pharyngeal valve,
465 transforming feeding motions into spitting motions. The pm3s make up the bulk of the
466 anterior pharynx, which pumps rhythmically during spitting. Opening of the pharyngeal
467 valve by the pm3s requires that a subcellular compartment at the anterior end of the
468 pm3s undergoes a sustained uncoupling from the rest of the cell and stay contracted.
469 Strikingly, the remaining posterior portion of each pm3 muscle cell continues to pump,
470 ejecting material. The subcellular contraction of the pm3s is accompanied by localized
471 increases in intracellular muscle calcium at the site of the pharyngeal valve. Spitting
472 behavior, opening of the metastomal filter, and muscle calcium physiology are
473 controlled by the M1 neuron, which directly innervates the pharyngeal muscles that
474 control the filter and valve. The gustatory-receptor orthologs *lite-1* and *gur-3* function
475 redundantly in the control of light-induced spitting: *lite-1* plays a major role and suffices
476 for nearly wild-type responses to light, while *gur-3* plays a smaller role and is sufficient
477 to partially open the valve and filter but not to increase pumping rate. *gur-3* functions in
478 the I2 pharyngeal neurons and likely also in the I4 neuron to evoke this attenuated
479 spitting response via the M1 neuron.
480

481 **Subcellular muscle units driven by neuronally regulated subcellularly localized**
482 **calcium signaling modulate motor behavior**

483 We identified a likely physiological effector for the subcellular muscle contraction of the
484 pm3s: calcium transients in pharyngeal muscle that colocalize with the specific muscle
485 region that undergoes sustained contraction during spitting and from which the
486 pharyngeal valve protrudes. We propose that these calcium transients are the drivers of
487 the subcellular muscle contraction of the pm3s.

488 Subcellularly localized calcium signaling in muscle has been observed in other
489 systems. Subcellular muscle calcium transients known as “calcium sparks” result from
490 calcium influx via individual ryanodine receptors (Cheng *et al*., 1993). These localized
491 calcium increases can trigger calcium-induced calcium release from the sarcoplasmic
492 reticulum, resulting in a wave of calcium release that drives excitation-contraction
493 coupling (Cheng *et al*., 1993; Kuo and Ehrlich, 2015). Calcium sparks also allow local
494 increases in intracellular calcium to drive nearby signaling events without elevating
495 global calcium levels (Nelson *et al*., 1995; Navedo *et al*., 2005; Nieves-Cintrón *et al*.,
496 2008).

497 Despite these examples of localized calcium in muscle in physiological settings,
498 how subcellular muscle calcium signaling contributes to behavior is poorly understood.
499 The *C. elegans* pm5 pharyngeal muscle cells function to swallow food from the anterior
500 pharynx to the terminal bulb via a peristaltic wave of subcellular contraction (Avery and
501 Horvitz, 1987), and subcellular calcium signals in the pm5s likely underlie swallowing
502 behavior (Shimozono *et al*., 2004; Kozlova *et al*., 2019). These transients have been
503 proposed to resemble calcium waves in cardiac muscle (Kozlova *et al*., 2019), a

504 phenomenon driven by the propagation of calcium-induced calcium release from
505 internal stores (Cheng *et al*., 1993). Subcellular signals have also been observed in
506 enteric muscles, which can contract peristaltically, but the functional significance of
507 these signals is unknown (Yamazawa and Iino, 2002). Our results identify a different
508 and novel role for subcellular muscle contraction and calcium signaling: sustained,
509 neuronally induced contraction of a stable, dedicated subcompartment of muscle, thus
510 modulating function and transforming one behavioral output into another. While calcium
511 sparks and *C. elegans* peristalsis behavior occur on a timescale of tens of milliseconds,
512 the contractions and calcium signals that we observed can last at least 10 seconds.
513 This timescale is more similar to that of calcium sparklets produced by L-type voltage-
514 gated calcium channels (Navedo *et al*., 2005). We propose that subcellular muscle
515 contraction via subcellular calcium signaling is a mechanism by which the nervous
516 system can modulate muscle function to alter motor outputs and so generate distinct
517 behaviors, and further suggest that *C. elegans* spitting behavior offers a system for the
518 analysis of the molecular bases of subcellular calcium signaling in muscle using a highly
519 genetically tractable organism.
520

521 **Independent control of the pharyngeal valve and metastomal filter generates four**
522 **distinct pumping behaviors**

523 We observed that, in addition to opening the pharyngeal valve, spitting worms open the
524 metastomal filter and that this opening depends in part on the pm2 muscles. This finding

525 suggests that in addition to passively filtering incoming material as reported previously
526 (Fang-Yen *et al*., 2009), the metastomal filter can be actively opened to allow
527 unrestricted entry of material into the pharynx. In the context of spitting pumps, opening
528 the filter permits new material to be rinsed in and out, while closing the filter allows
529 egestion without rinsing. We observed that the filter sometimes also opens during
530 feeding, producing “gulps” with greatly increased intake. Thus, the independent control
531 of the metastomal filter and pharyngeal valve produces four distinct pumping behavior
532 variants -- feeding, gulping, spitting with rinsing, and spitting without rinsing. Given that
533 M1 is the major source of innervation of the pm1 and pm2 muscles, from which the
534 metastomal filter protrudes (Albertson and Thomson, 1976), we think it likely that M1
535 can function in the production of gulps by opening the metastomal filter without
536 producing an accompanying contraction in the regions of pm3 that open the pharyngeal
537 valve. Such a behavior might allow enhanced consumption of certain preferred food or,
538 because it draws large amounts of material into the mouth, might allow the worm to
539 more efficiently sample the environment while foraging. The possibility that a single
540 neuron might control opposite behaviors (i.e., spitting and gulping) via the differential
541 activation of multiple downstream muscles and subcellular muscle compartments is
542 intriguing.
543
544 **The M1 neuron drives spitting from the waist of an hourglass circuit motif**

545 Our circuit studies show that the motor neuron M1 is a key regulator of spitting. We
546 speculate that in addition to controlling the muscles that produce spitting, M1 functions
547 as a central integrator of noxious taste information in the pharyngeal nervous system.
548 Several lines of evidence support this hypothesis. A recent analysis of the pharyngeal
549 connectome found that M1 exhibits a prominent and highly connected position in the
550 pharyngeal network (Cook *et al*., 2019), suggesting that M1 plays an important role in
551 network function. Second, M1 is particularly well-positioned to integrate noxious taste
552 stimuli, as it receives direct inputs from each of the other five *lite-1-* and/or *gur-3-*
553 expressing pharyngeal neurons (i.e., the paired I2 and single I4, M4, M5, and MI
554 neurons) (Albertson and Thomson, 1976; Bhatla and Horvitz, 2015). Consistent with this
555 reported connectivity, we found that two of these neuron classes, the I2s and I4,
556 contribute to M1's activation by light. Third, it is likely that M1 is itself light- and ROS-
557 sensitive, as it expresses both *lite-1* (Bhatla and Horvitz, 2015) and *gur-3* (this study)
558 and we show here that it can respond robustly to light even when synaptic and humoral
559 inputs are substantially reduced or eliminated, respectively. For these reasons, we
560 propose that M1 sits at the narrow waist of an "hourglass" circuit motif (Figure 7B). In
561 this motif, multiple upstream parallel pathways converge on M1, which in turn makes
562 divergent outputs onto the multiple downstream muscle groups that control the discrete
563 motor outputs of the spitting reflex. Such an "hourglass" structure was recently
564 described in a theoretical analysis of the larger *C. elegans* non-pharyngeal nervous

565 system (Sabrin *et al*., 2020). We propose that the neuromuscular circuit we describe
566 here constitutes a miniature variation of an “hourglass” circuit organization.

567

568 **The magnitude of M1 activation by the I2 and I4 neurons evokes a distinct subset**
569 **of hourglass motor outputs**

570 We explored circuitry upstream of the M1 neuron and identified the I2 and I4 neurons as
571 likely sites of *gur-3* function in light-induced spitting. The I2s inhibit pumping in response
572 to light, and I4 was previously shown to be activated by light (Bhatla and Horvitz, 2015),
573 but no function for I4 had previously been reported. Because I4 expresses *gur-3* and
574 controls responses to light, we speculate that I4 is also a cellular receptor for light and
575 ROS. Interestingly, although the pharyngeal connectome and our data suggest that M1
576 acts as a bottleneck through which signals must pass to evoke spitting, the I2/I4 circuit
577 can selectively produce a subset of M1-dependent behaviors by weakly activating M1.
578 Weak *gur-3*-dependent stimulation of M1 is sufficient to open the pharyngeal valve and
579 metastomal filter, but not to increase pumping rates. Because UV light robustly activates
580 the I2s (Bhatla and Horvitz, 2015), the fact that the I2s activate M1 only weakly
581 suggests that their input to M1 is similarly weak. The weakness of this connection might
582 be a design feature of the pharyngeal nervous system, allowing strong activation of the
583 I2 neurons to be converted into weak activation of the M1 neuron, thereby producing an
584 attenuated variation of spitting. We speculate that I4 might function in a similar way, and
585 that the I2s and I4 serve as modules to trigger attenuated spitting, while input from other

586 cells and/or endogenous *lite-1* function in M1 produce spitting in a more robust manner,
587 enabling the pharyngeal nervous system to generate graded variations of the spitting
588 reflex and thus fine-tune its output to the environment. One problem that must be solved
589 by an hourglass circuit structure with one or a few cells in the bottleneck is how to
590 differentially evoke downstream outputs when all upstream inputs must be compressed
591 together at the hourglass waist. We suggest that the M1 spitting circuit illustrates a
592 simple solution to this problem: graded activation of M1 in the hourglass waist activates
593 progressively larger subsets of downstream outputs. Outputs of such a circuit can thus
594 be tuned by adjusting the magnitude of upstream inputs, allowing upstream neurons to
595 input additively if their connections to the bottleneck are equally weighted or to evoke a
596 subset of downstream outputs if they only weakly activate the bottleneck (as is the case
597 with the I2 neurons).

598 Previous studies showed that the I2s inhibit pumping and that M1 is required for
599 spitting (Bhatla and Horvitz, 2015; Bhatla *et al*., 2015). We found that in addition the I2s
600 can promote pumps (spitting pumps) and that M1 can inhibit pumping (it does so in the
601 recovery phase). Thus, each of these neuron classes can function in superficially
602 opposite ways in different contexts. Although it might seem counterproductive for a
603 given neuron to both promote and inhibit pumping, both of these outputs share the
604 effect of reducing food intake, since spitting pumps eject previously ingested food. We
605 suggest that these differentially timed inhibitory and excitatory neural inputs to
606 pharyngeal muscle allow the pharynx to generate a sequence of actions, first inhibiting

607 pumping and/or stimulating spitting to eject noxious material, then increasing pumping
608 rate and rinsing in the burst pumping phase if noxious stimulation continues, and finally
609 inhibiting all pumping, including spitting, as the animal flees the site of the noxious
610 encounter. Additionally, because spitting with an opened metastomal filter results in
611 rinsing new material into the pharynx, it might be maladaptive if spitting persists when
612 the animal is in a large region of noxious material; in this case, circuits promoting
613 inhibition on a longer timescale than spitting would serve to limit additional exposure to
614 noxious material.

615 More generally, we propose that subcellular muscle contraction mediated by
616 subcellularly localized muscle calcium signaling is a fundamental mechanism by which
617 nervous systems can reshape motor outputs and suggest that hourglass motifs might
618 function broadly in neuronal circuit organization for the production of complex adaptive
619 behavior in response to changing environments.

620

621 **Acknowledgments**

622 We thank N. An, R. Droste, S. Flavell, N. Ji, E. Jorgensen, R. Komuniecki, J. Meisel, S.
623 Mitani, M. Treinin, Addgene, and the *Caenorhabditis* Genetics Center, which is funded
624 by NIH Office of Research Infrastructure Programs (P40 OD010440), for strains and
625 reagents; and K. Boulias, V. Dwivedi, K. Burkhart, D. Ghosh, H. Johnsen, T. Littleton, J.

626 Meisel, C. Pender, P. Reddien, J. Saul, and Horvitz laboratory members for discussions
627 and advice.
628

629 **Competing interests:** The authors declare that no competing interests exist.

630 **Materials and methods**

631 ***C. elegans* strains and transgenes (listed in order of appearance):**

632 N2 (wild type)

633 CB1072 *unc-29(e1072)*

634 MT26279 *lin-15(n765ts); nIs507 [inx-4$_{promoter}$::GFP; lin-15(+)]*

635 MT23338 *nIs686 [gpa-16$_{promoter}$::gcamp3::unc-54 3' UTR; lin-15(+)] III; lin-15AB(n765ts)*

636 MT21783 *gur-3(ok2245)*

637 KG1180 *lite-1(ce314)*

638 MT21793 *lite-1(ce314) gur-3(ok2245)*

639 DA1113 *eat-2(ad1113)*

640 MT25982 *eat-2(ad1113); gur-3(ok2245)*

641 MT22899 *eat-2(ad1113); lite-1(ce314)*

642 MT25983 *eat-2(ad1113); lite-1(ce314) gur-3(ok2245)*

643 MT25999 *eat-2(ad1113); lite-1(ce314) gur-3(ok2245); nIs687 [lite-1$_{promoter}$::gfp::lite-1; lin-*

644 *15(+)]*

645 MT25809 *lite-1(ce314) gur-3(ok2245) lin-15(n765ts); nEx2281 [lite-1$_{promoter}$::lite-1::gfp;*

646 *lin-15(+)]*

647 MT25810 *lite-1(ce314) gur-3(ok2245) lin-15(n765ts); nEx2157 [gur-3 gDNA; lin-15(+)]*

648 MT23415 *nIs686 III; gur-3(ok2245) lin-15(n765ts)*

649 MT23417 *nIs686 III; lite-1(ce314) lin-15(n765ts)*

650 MT23370 *nIs686 III; lite-1(ce314) gur-3(ok2245) lin-15(n765ts)*

651 MT25631 *lin-15(n765ts); nIs864 [glr-2$_{promoter}$::gfp::unc-54 3' UTR; lin-15(+)]*

652 MT25732 *lin-15(n765ts); nIs864; nEx2905 [lury-1$_{promoter}$::ice::sl2::mcherry::unc-54 3'*
653 *UTR; ttx-3$_{promoter}$::mcherry]*

654 MT23192 *lin-15(n765ts); nIs678 [glr-2$_{promoter}$::gcamp6s::unc-54 3' UTR; lin-15(+)]*

655 MT23250 *gur-3(ok2245) lin-15(n765ts); nIs678*

656 MT23230 *lite-1(ce314) lin-15(n765ts); nIs678*

657 MT23369 *lite-1(ce314) gur-3(ok2245) lin-15(n765ts); nIs678*

658 MT23343 *unc-13(s69); lin-15(n765ts); nIs678*

659 MT23410 *unc-31(u280); lin-15(n765ts); nIs678*

660 MT25468 *lite-1(ce314) gur-3(ok2245) lin-15(n765ts); nEx2815 [lury-*
661 *1$_{promoter}$::chr2::sl2::mcherry::unc-54 3' UTR]*

662 MT2360*6 lite-1(ce314) gur-3(ok2245) lin-15AB(n765ts); nEx2144 [flp-*
663 *15$_{promoter}$::mcherry::gur-3, lin-15(+)]*

664 MT23545 *lite-1(ce314) gur-3(ok2245) lin-15AB(n765ts); nIs678 ; nEx2144*

665 MT26001 *eat-2(ad1113); lite-1(ce314) gur-3(ok2245) nIs791 X [integrated transgene*
666 *derived from nEx2144: flp-15$_{promoter}$::mcherry::gur-3, lin-15(+)]*

667 MT21421 *nIs569 [flp-15$_{promoter}$::csp-1b; ges-1$_{promoter}$::gfp]*

668 MT21791 *lite-1(ce314) nIs569*

669

670 **Supplemental strains:**

671 MT2249 *egl-47(n1082dm)*

672 RB850 *egl-47(ok677)*

673 RB845 *gur-4(ok672)*

674 FX06169 *gur-5(tm6169)*

675 MT24110 *lin-15(n765ts); nIs780 [gur-3$_{promoter}$::gfp; lin-15(+)]*

676 MT25804 *oxIs322 [myo-2$_{promoter}$::mcherry::h2b; myo-3$_{promoter}$::mcherry::h2b] II ; nIs310*
677 *[nlp-13$_{promoter}$::gfp] V; nEx2905*

678 MT25950 *eat-2(ad1113); nIs865 [integrated transgene derived from nEx2905: lury-*
679 *1$_{promoter}$::ice::sl2::mcherry::unc-54 3' UTR; ttx-3$_{promoter}$::mcherry]*

680 CB933 *unc-17(e245)*

681 PR1152 *cha-1(p1152)*

682 RM509 *ric-3(md158)*

683 CB156 *unc-25(e156) dnj-17(ju1162)*

684 MT6308 *eat-4(ky5)*

685 CB1112 *cat-2(e1112)*

686 MT10661 *tdc-1(n3420)*

687 MT14984 *tph-1(n4622)*

688 MT15434 *tph-1(mg280)*

689 MT22280 *ser-4(ok512); mod-1(ok103); ser-1(ok345) ser-7(tm1325)*

690 CB211 *lev-1(e211)*

691 MT6637 *acr-2(n2595 n2420)*

692 RB1659 *acr-3(ok2049)*

693 TU1803 *deg-3(u662) des-2(u695)*

694 NC293 *acr-5(ok180)*

695 FX03723 *acr-6(tm3723)*

696 FX863 *acr-7(tm863)*

697 RB1195 *acr-8(ok1240)*

698 FX02515 *acr-10(tm2515)*

699 VC40816 *acr-11(gk827759)*

700 VC188 *acr-12(ok367)*

701 ZZ15 *lev-8/acr-13(x15)*

702 FX05819 *acr-14(tm5819)*

703 RB1172 *acr-15(ok1214)*

704 RB918 *acr-16(ok789)*

705 VC40773 *acr-17(gk804825)*

706 VC40487 *acr-17(gk661490)*

707 VC20403 *acr-18(gk324494)*

708 VC491 *acr-19(ok967)*

709 VC20325 *acr-20(gk161737)*

710 RB1250 *acr-21(ok1314)*

711 VC20417 *acr-23(gk231233)*

712 EG8095 *acr-23(ox429)*

713 RB2119 *acr-23(ok2804)*

714 VC20738 *acr-24(gk387895)*

715 VC40292 *acr-24(gk557791)*

716 MT21980 *deg-3(u773)*

717 CB904 *unc-38(e264)*

718 MT1512 *lev-7/unc-63(x13)*

719 FX03268 *acc-1(tm3268)*

720 VC40182 *acc-2(gk501637)*

721 VC1757 *acc-2(ok2216)*

722 FX03219 *acc-2(tm3219)*

723 FX03174 *acc-3(tm3174)*

724 CX12724 *acc-4(ok2371)*

725 MT22153 *lgc-40(tm3377)*

726 VC20746 *pbo-5(gk963058)*

727 RB1379 *pbo-6(ok1564)*

728 RB896 *gar-1(ok755)*

729 RB756 *gar-2(ok520)*

730 VC670 *gar-3(gk337)*

731

732 **Molecular biology**

733 Transgenes were generated by standard cloning methods. DNA sequences used in the

734 generation of transgenes were amplified with the primers indicated below.

735

736 Generated using the infusion cloning technique (Takara Bio, Mountain View, CA) and

737 injected as plasmids:

738 *nIs864 - pSS028 [glr-2$_{promoter}$::gfp::unc-54 3' UTR]*

739 *nEx2905 and nIs865 - pSS042 [lury-1$_{promoter}$::ice::sl2::mcherry::unc-54 3' UTR]*

740 *nEx2815 - pSS034 [lury-1$_{promoter}$::chr2::sl2::mcherry::unc-54 3' UTR]*

741

742 *glr-2$_{promoter}$*: TTGGGACAAATGTGGAAACGA,

743 TTCGCTTTTTACAGAGTTAACTCTGC

744 *lury-1$_{promoter}$*: TTCATTAAGTAATCCGTTTAGGGCAAAT,

745 GATTGGATTTTCTGGAATAATCGGGT

746 *ice*: ATGGCCGACAAGGTCCTGA,

747 TTAATGTCCTGGGAAGAGGTAGAAACATC

748

749 Generated and injected as PCR product*:*

750 *nIs686 - pcNB1 [gpa-16$_{promoter}$::gcamp3::unc-54 3' UTR]*

751 *nEx2157 – pcNB20 [gur-3$_{promoter}$::gur-3 gDNA::gur-3 3' UTR]*

752 *nIs678 - [glr-2$_{promoter}$::gcamp6s::unc-54 3' UTR]*

753

754 *gpa-16*$_{promoter}$: ACCAACCTGAACAGCGAATC,

755 AAAGGGAATTTTATGTGAATAATATCG

756 *gur-3*$_{promoter}$*::gur-3 gDNA::gur-3 3' UTR:* GCCTGATGGAACACACTTCCAAC

757 GTTTACCCCGTCTCTATTTCCGCTTTG

758 *gcamp6s*: ATGGGTTCTCATCATCATCATCATC,

759 GCCCGTACGGCCGACTAGTAGG

760

761 **Grinder Pumping Assay**

762 Previously, we used a xenon bulb (Till Photonics Polychrome V, 150 W; Thermo Fischer
763 Scientific, Waltham, MA) to deliver 365 nm UV light through an inverted microscope
764 (Axiovert S100; Zeiss, Oberkochen, Germany) to individual worms on an agar pad
765 (Bhatla and Horvitz, 2015). Because of the low throughput of this approach, we
766 designed a device to deliver 365 nm UV light to standard Petri dishes used for culturing
767 worms and used this apparatus to assay behavioral responses to 365 nm UV light as
768 described previously for 436 nm violet light (Bhatla and Horvitz, 2015). The apparatus
769 consists of a UV-light-emitting LED (M365F1; Thorlabs, Newton, NJ) coupled by a fiber-
770 optic cable to a collimating lens. The LED system delivers 365 nm UV light in a 3-4 mm
771 spot at a power of ~1.5mW/mm$^2$ to young (1-day post-L4) hermaphrodite adults moving
772 freely on a Petri dish, producing a burst pumping response indistinguishable from that
773 obtained previously (Bhatla and Horvitz, 2015). Custom Matlab software was used to

774 control the LED, and the contraction rate of the grinder before, during, and after
775 application of light was observed by eye via a dissecting microscope and manually
776 recorded via this software (Bhatla and Horvitz, 2015). All behavioral data were
777 visualized as described in (Bhatla and Horvitz, 2015; Bhatla *et al*., 2015). All behavioral
778 assays and imaging experiments were performed in the same location, at which
779 temperature averaged 19°C, with a standard deviation of 1.2°C.
780

781 **Pharyngeal transport assay**

782 Pharyngeal transport assays were performed as described previously (Bhatla *et al*.,
783 2015). To visualize the direction of flow in the pharynx during each pump, worms were
784 fed a 50% dilution of 1 µm polystyrene beads (Polysciences, Warrington, PA) in M9
785 buffer. Young (1-day post-L4) hermaphrodite adults were placed with bacteria on an
786 NGM agar pad on a coverslip and observed with a 20x objective on an inverted
787 microscope (Axiovert S100; Zeiss). Videos were recorded at 1000 frames per sec using
788 a high-speed video camera (Fastcam Mini; Photron, Tokyo, Japan). 365 nm UV light
789 (0.88-1.5 mW/mm$^2$) was presented to the worm for 10 sec (Till Photonics Polychrome V,
790 150 W xenon bulb; Thermo Fischer Scientific). Hydrogen peroxide was administered as
791 described previously (Bhatla and Horvitz, 2015). Videos were viewed and manually
792 annotated, using custom Matlab software, for specific behavioral events: ingestion
793 (beads being retained in the procorpus after procorpus relaxation), spitting (beads
794 flowing out of the procorpus), and pumping (movement of the grinder). In some cases,

795 the worm moved temporarily out of the focal plane of the microscope or field-of-view of
796 the camera. These unscorable frames were annotated as "missing" and excluded from
797 further analysis. The position of the metastomal filter was scored separately based on
798 whether beads passed freely through or accumulated in the buccal cavity during feeding
799 or spitting, and the fraction of feeding and spitting pumps with the filter open or closed
800 was calculated for the period before and during illumination. Animals with fewer than
801 five scorable pumps in a given 10 sec interval were censored from these analyses.

802

803 **Muscle motion visualization assay**

804 To visualize the timing of pharyngeal muscle motions during each pump, young (1-day
805 post-L4) hermaphrodite adults were placed with bacteria on an NGM agar pad
806 underneath a coverslip and observed with a 20x objective on an inverted microscope
807 (Axiovert S100; Zeiss ). Videos were recorded at 86 frames per sec using an EMCCD
808 camera (iXon$^{+}$; Andor, Belfast, United Kingdom). 365 nm UV light was presented to the
809 worm for 10 sec (Till Photonics Polychrome V, 150 W xenon bulb; Thermo Fischer
810 Scientific). Slow-moving *unc-29(e1072)* animals were filmed to facilitate video capture.
811 Videos were viewed and manually annotated based on whether the anterior tip of the
812 pharynx closed or remained open at the end of each pump.

813

814 **Laser ablations**

815 We used a pulsed nitrogen laser (MicroPoint; Andor) coupled to a compound
816 microscope (Axioplan; Zeiss) to conduct laser microsurgery of individual pharyngeal
817 neurons, as previously described (Fang-Yen *et al*., 2012). Briefly, worms were
818 immobilized using 10 mM sodium azide and mounted for viewing through a 100x oil
819 objective. Ablations were performed on hermaphrodite larvae of stages 1 or 2 (L1 or
820 L2), with cell nuclei identified by either Nomarski differential interference contrast optics
821 or cell-specific GFP reporters. Specifically, M1 was identified by Nomarski optics or by
822 the M1-expressed GFP reporter *nIs864*, which drives expression of GFP in M1 via the
823 *glr-2* promoter (Brockie *et al*., 2001), while pm1 was identified by GFP reporter *nIs507*,
824 which drives expression of GFP in pm1 via the *inx-4* promoter (Altun *et al*., 2009). The
825 pm2 muscles, the I2 and I4 neurons, and, in some experiments, the M1 neuron were
826 identified by Nomarski optics. Ablations were confirmed the following day by
827 appearance under Nomarski optics and/or by the loss of cell-specific fluorescence. On
828 day 3 or 4, adults were assayed for their response to light. Mock-ablated animals were
829 mounted alongside ablation animals and received identical treatments (i.e., observation
830 of nuclear morphology and/or GFP expression) at each step. Animals were allocated
831 into mock and ablation groups randomly.

832

833 **Genetic ablation**

834 M1 was ablated genetically by overexpressing the mammalian caspase ICE fused to an
835 *sl2::mcherry* sequence in M1 driven by the *lury-1* promoter (Ohno *et al*., 2017). For all

836 animals assayed, genetic ablation of M1 was confirmed beforehand using an M1-
837 specific GFP marker *(nIs864)*, which drives expression of GFP in M1 via the *glr-2*
838 promoter (Brockie *et al*., 2001). The *nEx2905* genetic ablation transgene also killed the
839 M2 neurons in approximately 50% of animals assayed (Figure S4A), as confirmed using
840 an M2-specific GFP marker (*nIs310*) (Luo and Horvitz, 2017). The *sl2::mcherry*
841 sequence used drove varying degrees of mCherry expression in pharyngeal muscle,
842 and we found that the brightness of this mCherry expression correlated with the rate of
843 M2-killing, such that selecting animals with dim pharyngeal mCherry expression
844 reduced the rate of M2-killing to 1-2% (Figure S4C). Animals assayed in Figure 4D and
845 4E were not selected in this way. We did not determine the rate of M1 or M2 killing in
846 *nIs865* animals.

847

848 **Optogenetic depolarization**

849 Optogenetic manipulations were performed as described previously (Bhatla *et al.*,
850 2015). Cultivation plates were seeded with 300 µL of OP50 *E. coli* mixed with 0.5 µL of
851 100 mM all-*trans* retinal (ATR+) or ethanol alone (ATR-) and stored in the dark.
852 Transgenic hermaphrodite worms carrying the channelrhodopsin 2 (*chr2*) coding
853 sequence (Nagel *et al*., 2003; Boyden *et al*., 2005) fused to a *sl2::mcherry* sequence
854 were cultivated on these plates in the dark from egg to adulthood. For behavioral
855 assays, one-day-old animals were analyzed as described above ('Pharyngeal Transport
856 Assay'), except that 470 nm light was used in the place of 365 nm UV light. *nEx2815*

857 *[lury-1$_{promoter}$::chr2::sl2::mcherry::unc-54 3' UTR]* was expressed in both M1 and the M2s
858 driven by the *lury-1* promoter (Ohno *et al*., 2017). To avoid confounding optogenetic
859 activation of the M2s, we assayed only mosaic animals pre-selected for expression of
860 mCherry in M1 but not the M2s. Animals were allocated into ATR- and ATR+ groups
861 randomly.

862

863 **Calcium imaging**

864 Calcium imaging was performed as described previously (Bhatla and Horvitz, 2015).
865 Cellular calcium changes were monitored using either GCaMP3 (Tian *et al*., 2009)
866 expressed using the *nIs686* transgene in pharyngeal muscle driven by the *gpa-16*
867 promoter (Jansen *et al*., 1999) or GCaMP6s (Chen *et al*., 2013) expressed in M1 using
868 the *nIs678* transgene driven by the *glr-2* promoter (Brockie *et al*., 2001). Adult
869 hermaphrodite worms were immobilized using polystyrene beads on 10% agarose pads
870 under a coverslip (Kim *et al*., 2013a), and neurons were imaged using an inverted
871 microscope (Axiovert S100; Zeiss) with a 40x air objective. To stimulate animals with
872 UV light and image GCaMP fluorescence simultaneously, light was flickered between
873 365 nm UV and 485 nm light at a rate of 2 Hz. Behavioral spitting responses to flickered
874 365 nm / 485 nm light were indistinguishable from behavioral responses to 365 nm light
875 (not shown). Videos were recorded using an EMCCD camera (iXon$^{+}$; Andor) and
876 analyzed using custom Matlab software as described previously (Bhatla and Horvitz,
877 2015; Bhatla *et al.*, 2015). The immobilized pumping assay described in Figure S2A

878 was performed under the same conditions described above for calcium imaging, with
879 the exception that animals were stimulated with only 485 nm light.

880

881 **Behavioral Statistics**

882 For all measurements, each animal was scored once. Biological replicates were
883 performed using separate populations of animals on different days and consisted of 20
884 animals unless indicated otherwise. Statistics for significance of differences between
885 fractions in metastomal filter analyses were calculated as follows. Fractions were log-
886 transformed, and any fractions with a numerator of zero were approximated to 0.1 prior
887 to transformation. Similar results were obtained by approximating numerators of zero
888 with 0.01. Log-transformed datasets were assessed for significance with an unpaired t-
889 test when a single pair of conditions was compared or unpaired ordinary one-way
890 ANOVA analysis when multiple conditions were compared. These analyses assumed
891 that log-transformed data followed a normal distribution with similar standard deviations.
892 Statistics for significance between average spitting rates were calculated as follows. For
893 each animal, the total number of spits observed during stimulation with light was divided
894 by the number of scorable frames in the light administration phase for that animal to
895 give the average pumping rate during light administration. Significance of differences
896 between groups was assessed by unpaired, ordinary one-way ANOVA analysis, with
897 the assumption that the data followed a Gaussian distribution with similar standard
898 deviations. Pumping inhibition was calculated by dividing the average pumping rate

899 during light stimulation (10 < t < 20) by the average pumping rate in the feeding phase
900 (0 < t <10). All statistics were calculated using Prism (GraphPad Software, San Diego,
901 CA).

902

903 **Author contributions**

904 SRS - Conceptualization, Methodology, Investigation, Resources, Formal analysis,
905 Validation, Writing (original draft), Writing (reviewing and editing), Visualization

906 NB - Conceptualization, Methodology, Investigation, Resources, Formal analysis,
907 Writing (reviewing and editing)

908 ELLQ - Formal analysis, Writing (reviewing and editing)

909 HRH - Conceptualization, Writing (reviewing and editing), Supervision, Funding
910 Acquisition

## References


Albertson, D.G., and Thomson, J.N. (1976). The pharynx of *Caenorhabditis elegans*. Philosophical Transactions of the Royal Society of London. B, Biological Sciences *275*, 299–325.

Altun, Z.F., Chen, B., Wang, Z.W., and Hall, D.H. (2009). High resolution map of *Caenorhabditis elegans* gap junction proteins. Developmental Dynamics *238*, 1936–1950.

Arenas, O.M., Zaharieva, E.E., Para, A., Vásquez-Doorman, C., Petersen, C.P., and Gallio, M. (2017). Activation of planarian TRPA1 by reactive oxygen species reveals a conserved mechanism for animal nociception. Nat Neurosci *20*, 1686–1693.

Avery, L. (1993). Motor neuron M3 controls pharyngeal muscle relaxation timing in *Caenorhabditis elegans*. Journal of Experimental Biology *175*, 283–297.

Avery, L., and Horvitz, H.R. (1987). A cell that dies during wild-type *C. elegans* development can function as a neuron in a *ced-3* mutant. Cell *51*, 1071–1078.

Avery, L., and Horvitz, H.R. (1989). Pharyngeal pumping continues after laser killing of the pharyngeal nervous system of *C. elegans*. Neuron *3*, 473–485.

Avery, L., and You, Y. (2012). *C. elegans* feeding. WormBook, ed. The *C. elegans* Research Community, WormBook, doi/10.1895/wormbook.1.150.1, http://www.wormbook.org.

Berwin, B., Floor, E., and Martin, T.F.J. (1998). CAPS (mammalian UNC-31) protein localizes to membranes involved in dense-core vesicle exocytosis. Neuron *21*, 137–145.

Bhatla, N., and Horvitz, H.R. (2015). Light and hydrogen peroxide inhibit *C. elegans* feeding through gustatory receptor orthologs and pharyngeal neurons. Neuron *85*, 804–818.

Bhatla, N., Droste, R., Sando, S.R., Huang, A., and Horvitz, H.R. (2015). Distinct neural circuits control rhythm inhibition and spitting by the myogenic pharynx of *C. elegans*. Current Biology *25*, 2075–2089.

Birkholz, T.R., and Beane, W.S. (2017). The planarian TRPA1 homolog mediates extraocular behavioral responses to near-ultraviolet light. Journal of Experimental Biology *220*, 2616–2625.

Boyden, E.S., Zhang, F., Bamberg, E., Nagel, G., and Deisseroth, K. (2005). Millisecond-timescale, genetically targeted optical control of neural activity. Nat Neurosci *8*, 1263–1268.

Briggman, K.L., and Kristan, W.B. (2008). Multifunctional pattern-generating circuits. Annual Review of Neuroscience *31*, 271–294.

Brockie, P.J., Madsen, D.M., Zheng, Y., Mellem, J., and Maricq, A.V. (2001). Differential expression of glutamate receptor subunits in the nervous system of *Caenorhabditis elegans* and their regulation by the homeodomain protein UNC-42. J. Neurosci. *21*, 1510–1522.

952 Cerretti, D.P., Kozlosky, C.J., Mosley, B., Nelson, N., Ness, K.V., Greenstreet, T.A.,
953 March, C.J., Kronheim, Druck, T., Cannizzaro, L.A., *et al*. (1992). Molecular
954 cloning of the interleukin-1 beta converting enzyme. Science *256*, 97–100.
955 Chen, T., Wardill, T.J., Sun, Y., Pulver, S.R., Renninger, S.L., Baohan, A., Schreiter,
956 E.R., Kerr, R.A., Orger, M.B., Jayaraman, V., *et al*. (2013). Ultrasensitive
957 fluorescent proteins for imaging neuronal activity. Nature *499*, 295–300.
958 Cheng, H., Lederer, W., and Cannell, M. (1993). Calcium sparks: elementary events
959 underlying excitation-contraction coupling in heart muscle. Science *262*, 740–
960 744.
961 Cook, S.J., Crouse, C.M., Yemini, E., Hall, D.H., Emmons, S.W., and Hobert, O. (2019).
962 The connectome of the *Caenorhabditis elegans* pharynx. BioRxiv
963 https://doi.org/10.1101/868513.
964 Dent, J.A., Smith, M.M., Vassilatis, D.K., and Avery, L. (2000). The genetics of
965 ivermectin resistance in *Caenorhabditis elegans*. PNAS *97*, 2674–2679.
966 Du, E.J., Ahn, T.J., Wen, X., Seo, D.-W., Na, D.L., Kwon, J.Y., Choi, M., Kim, H., Cho,
967 H., and Kang, K. (2016). Nucleophile sensitivity of *Drosophila* TRPA1 underlies
968 light-induced feeding deterrence. eLife *5*, e18425.
969 Edwards, S.L., Charlie, N.K., Milfort, M.C., Brown, B.S., Gravlin, C.N., Knecht, J.E., and
970 Miller, K.G. (2008). A novel molecular solution for ultraviolet light detection in
971 *Caenorhabditis elegans*. PLOS Biology *6*, e198.
972 Fang-Yen, C., Avery, L., and Samuel, A.D.T. (2009). Two size-selective mechanisms
973 specifically trap bacteria-sized food particles in *Caenorhabditis elegans*. PNAS
974 *106*, 20093–20096.
975 Fang-Yen, C., Gabel, C.V., Samuel, A.D.T., Bargmann, C.I., and Avery, L. (2012). Laser
976 microsurgery in *Caenorhabditis elegans*. In Methods in Cell Biology, (Elsevier),
977 pp. 177–206.
978 Flavell, S.W., Pokala, N., Macosko, E.Z., Albrecht, D.R., Larsch, J., and Bargmann, C.I.
979 (2013). Serotonin and the neuropeptide PDF initiate and extend opposing
980 behavioral states in *C. elegans*. Cell *154*, 1023–1035.
981 Franks, C.J., Murray, C., Ogden, D., O'Connor, V., and Holden-Dye, L. (2009). A
982 comparison of electrically evoked and channel rhodopsin-evoked postsynaptic
983 potentials in the pharyngeal system of *Caenorhabditis elegans*. Invert Neurosci *9*,
984 43–56.
985 Guntur, A.R., Gu, P., Takle, K., Chen, J., Xiang, Y., and Yang, C. (2015). *Drosophila*
986 TRPA1 isoforms detect UV light via photochemical production of $H_2O_2$. Proc Natl
987 Acad Sci USA *112*, E5753–E5761.
988 Guntur, A.R., Gou, B., Gu, P., He, R., Stern, U., Xiang, Y., and Yang, C. (2017). $H_2O_2$-
989 sensitive isoforms of *Drosophila melanogaster* TRPA1 act in bitter-sensing
990 gustatory neurons to promote avoidance of UV during egg-laying. Genetics *205*,
991 749–759.

992 Halevi, S., McKay, J., Palfreyman, M., Yassin, L., Eshel, M., Jorgensen, E., and Treinin,
993 M. (2002). The *C. elegans ric-3* gene is required for maturation of nicotinic
994 acetylcholine receptors. The EMBO Journal *21*, 1012–1020.
995 Hill, K., and Schaefer, M. (2009). Ultraviolet light and photosensitising agents activate
996 TRPA1 via generation of oxidative stress. Cell Calcium *45*, 155–164.
997 Jansen, G., Thijssen, K.L., Werner, P., van der Horst, M., Hazendonk, E., and Plasterk,
998 R.H.A. (1999). The complete family of genes encoding G proteins of
999 *Caenorhabditis elegans*. Nature Genetics *21*, 414.
1000 Kerr, R., Lev-Ram, V., Baird, G., Vincent, P., Tsien, R.Y., and Schafer, W.R. (2000).
1001 Optical imaging of calcium transients in neurons and pharyngeal muscle of *C.*
1002 *elegans*. Neuron *26*, 583–594.
1003 Kim, M.J., and Johnson, W.A. (2014). ROS-mediated activation of *Drosophila* larval
1004 nociceptor neurons by UVC irradiation. BMC Neurosci *15*, 14.
1005 Kim, E., Sun, L., Gabel, C.V., and Fang-Yen, C. (2013a). Long-term imaging of
1006 *Caenorhabditis elegans* using nanoparticle-mediated immobilization. PLoS ONE
1007 *8*, e53419.
1008 Kim, M.J., Ainsley, J.A., Carder, J.W., and Johnson, W.A. (2013b). Hyperoxia-triggered
1009 aversion behavior in *Drosophila* foraging larvae is mediated by sensory detection
1010 of hydrogen peroxide. Journal of Neurogenetics *27*, 151–162.
1011 Kohn, R.E., Duerr, J.S., McManus, J.R., Duke, A., Rakow, T.L., Maruyama, H., Moulder,
1012 G., Maruyama, I.N., Barstead, R.J., and Rand, J.B. (2000). Expression of
1013 Multiple UNC-13 Proteins in the *Caenorhabditis elegans* Nervous System. Mol
1014 Biol Cell *11*, 3441–3452.
1015 Kozlova, A.A., Lotfi, M., and Okkema, P.G. (2019). Crosstalk with the GAR-3 Receptor
1016 Contributes to Feeding Defects in *Caenorhabditis elegans eat-2* Mutants.
1017 Genetics *212*, 231–243.
1018 Kuo, I.Y., and Ehrlich, B.E. (2015). Signaling in muscle contraction. Cold Spring Harb
1019 Perspect Biol *7*, :a006023.
1020 Li, Z., Li, Y., Yi, Y., Huang, W., Yang, S., Niu, W., Zhang, L., Xu, Z., Qu, A., Wu, Z., *et*
1021 *al*. (2012). Dissecting a central flip-flop circuit that integrates contradictory
1022 sensory cues in *C. elegans* feeding regulation. Nature Communications *3*, 1–8.
1023 Liu, J., Ward, A., Gao, J., Dong, Y., Nishio, N., Inada, H., Kang, L., Yu, Y., Ma, D., Xu,
1024 T., *et al*. (2010). *C. elegans* phototransduction requires a G protein–dependent
1025 cGMP pathway and a taste receptor homolog. Nature Neuroscience *13*, 715–
1026 722.
1027 Luo, S., and Horvitz, H.R. (2017). The CDK8 complex and proneural proteins together
1028 drive neurogenesis from a mesodermal lineage. Current Biology *27*, 661–672.
1029 Marder, E., and Calabrese, R.L. (1996). Principles of rhythmic motor pattern generation.
1030 Physiological Reviews *76*, 687–717.
1031 Maruyama, I.N., and Brenner, S. (1991). A phorbol ester/diacylglycerol-binding protein
1032 encoded by the *unc-13* gene of *Caenorhabditis elegans*. PNAS *88*, 5729–5733.

1033 Nagel, G., Szellas, T., Huhn, W., Kateriya, S., Adeishvili, N., Berthold, P., Ollig, D.,
1034 Hegemann, P., and Bamberg, E. (2003). Channelrhodopsin-2, a directly light-
1035 gated cation-selective membrane channel. PNAS *100*, 13940–13945.
1036 Navedo, M.F., Amberg, G.C., Votaw, V.S., and Santana, L.F. (2005). Constitutively
1037 active L-type $Ca^{2+}$ channels. Proceedings of the National Academy of Sciences
1038 *102*, 11112–11117.
1039 Nelson, M.T., Cheng, H., Rubart, M., Santana, L.F., Bonev, A.D., Knot, H.J., and
1040 Lederer, W.J. (1995). Relaxation of arterial smooth muscle by calcium sparks.
1041 Science *270*, 633–637.
1042 Nieves-Cintrón, M., Amberg, G.C., Navedo, M.F., Molkentin, J.D., and Santana, L.F.
1043 (2008). The control of $Ca^{2+}$ influx and NFATc3 signaling in arterial smooth muscle
1044 during hypertension. PNAS *105*, 15623–15628.
1045 Ohno, H., Yoshida, M., Sato, T., Kato, J., Miyazato, M., Kojima, M., Ida, T., and Iino, Y.
1046 (2017). Luqin-like RYamide peptides regulate food-evoked responses in *C.*
1047 *elegans*. eLife *6*, e28877.
1048 O'Sullivan, A., Lindsay, T., Prudnikova, A., Erdi, B., Dickinson, M., and von Philipsborn,
1049 A.C. (2018). Multifunctional wing motor control of song and flight. Current Biology
1050 *28*, 2705-2717.e4.
1051 Raizen, D.M., Lee, R.Y., and Avery, L. (1995). Interacting genes required for pharyngeal
1052 excitation by motor neuron MC in *Caenorhabditis elegans*. Genetics *141*, 1365–
1053 1382.
1054 Rhoades, J.L., Nelson, J.C., Nwabudike, I., Yu, S.K., McLachlan, I.G., Madan, G.K.,
1055 Abebe, E., Powers, J.R., Colón-Ramos, D.A., and Flavell, S.W. (2019). ASICs
1056 mediate food responses in an enteric serotonergic neuron that controls foraging
1057 behaviors. Cell *176*, 85-97.e14.
1058 Richmond, J.E., Davis, W.S., and Jorgensen, E.M. (1999). UNC-13 is required for
1059 synaptic vesicle fusion in *C. elegans*. Nat Neurosci *2*, 959–964.
1060 Richmond, J.E., Weimer, R.M., and Jorgensen, E.M. (2001). An open form of syntaxin
1061 bypasses the requirement for UNC-13 in vesicle priming. Nature *412*, 338–341.
1062 Sabrin, K.M., Wei, Y., Heuvel, M.P. van den, and Dovrolis, C. (2020). The hourglass
1063 organization of the *Caenorhabditis elegans* connectome. PLOS Computational
1064 Biology *16*, e1007526.
1065 Sawin, E.R., Ranganathan, R., and Horvitz, H.R. (2000). *C. elegans* locomotory rate is
1066 modulated by the environment through a dopaminergic pathway and by
1067 experience through a serotonergic pathway. Neuron *26*, 619–631.
1068 Shimozono, S., Fukano, T., Kimura, K.D., Mori, I., Kirino, Y., and Miyawaki, A. (2004).
1069 Slow $Ca^{2+}$ dynamics in pharyngeal muscles in *Caenorhabditis elegans* during
1070 fast pumping. EMBO Rep. *5*, 521–526.
1071 Speese, S., Petrie, M., Schuske, K., Ailion, M., Ann, K., Iwasaki, K., Jorgensen, E.M.,
1072 and Martin, T.F.J. (2007). UNC-31 (CAPS) is required for dense-core vesicle but
1073 not synaptic vesicle exocytosis in *Caenorhabditis elegans*. J. Neurosci. *27*,
1074 6150–6162.

1075 Taylor, S.R., Santpere, G., Reilly, M., Glenwinkel, L., Poff, A., McWhirter, R., Xu, C.,
1076 Weinreb, A., Basavaraju, M., Cook, S.J., *et al*. (2019). Expression profiling of the
1077 mature *C. elegans* nervous system by single-cell RNA-Sequencing. BioRxiv
1078 https://doi.org/10.1101/737577.
1079 The *C. elegans* Deletion Mutant Consortium (2012). Large-scale screening for targeted
1080 knockouts in the *Caenorhabditis elegans* genome. G3: Genes, Genomes,
1081 Genetics *2*, 1415–1425.
1082 Thornberry, N.A., Bull, H.G., Calaycay, J.R., Chapman, K.T., Howard, A.D., Kostura,
1083 M.J., Miller, D.K., Molineaux, S.M., Weidner, J.R., Aunins, J., *et al*. (1992). A
1084 novel heterodimeric cysteine protease is required for interleukin-1β processing in
1085 monocytes. Nature *356*, 768.
1086 Tian, L., Hires, S.A., Mao, T., Huber, D., Chiappe, M.E., Chalasani, S.H., Petreanu, L.,
1087 Akerboom, J., McKinney, S.A., Schreiter, E.R., *et al*. (2009). Imaging neural
1088 activity in worms, flies and mice with improved GCaMP calcium indicators.
1089 Nature Methods *6*, 875–881.
1090 Trojanowski, N.F., Padovan-Merhar, O., Raizen, D.M., and Fang-Yen, C. (2014). Neural
1091 and genetic degeneracy underlies *Caenorhabditis elegans* feeding behavior.
1092 Journal of Neurophysiology *112*, 951–961.
1093 Yamazawa, T., and Iino, M. (2002). Simultaneous imaging of $Ca^{2+}$ signals in interstitial
1094 cells of Cajal and longitudinal smooth muscle cells during rhythmic activity in
1095 mouse ileum. The Journal of Physiology *538*, 823–835.
1096 Zheng, Y., Brockie, P.J., Mellem, J.E., Madsen, D.M., and Maricq, A.V. (1999).
1097 Neuronal control of locomotion in *C. elegans* is modified by a dominant mutation
1098 in the GLR-1 ionotropic glutamate receptor. Neuron *24*, 347–361.
1099

1100 **Summary of figures and supplemental material**

1101

1102 **<u>Main figures:</u>**

1103 **Figure 1**

1104 **Figure 2**

1105 **Figure 3**

1106 **Figure 4**

1107 **Figure 5**

1108 **Figure 6**

1109 **Figure 7**

1110

1111 **<u>Supplemental material:</u>**

1112 **Figure 1—figure supplement 1**

1113 **Figure 2—figure supplement 1**

1114 **Figure 3—figure supplement 1**

1115 **Figure 4—figure supplement 1**

1116 **Figure 4—figure supplement 2**

1117 **Video 1**

1118 **Video 2**

1119 **Video 3**

1120 **Video 4**

1121 **Video 5**

1122 **Video 6**

1123 **Video 7**

1124 **Video 8**

1125 **Figure 1. Worms Spit as a Consequence of the Sustained Contraction of Anterior**
1126 **Pharyngeal Muscles**

1127 (A) Anatomy of the *C. elegans* pharynx; a, anterior; d, dorsal.

1128 (B) Grinder pumping response to 365 nm UV light (from Bhatla and Horvitz [2015]). Left,
1129 adult wild-type *C. elegans* head showing one pump of the grinder; center, raster plot of
1130 individual animals, each grinder contraction shown by a tick; right, backward moving
1131 average of the pumping rate of the same animals. Labels indicate the "acute inhibition,"
1132 "burst," and "recovery" phases of the response. Scale bar, 20 μm.

1133 (C) Representative images of worms feeding and spitting in the polystyrene bead
1134 feeding assay. Pumps were scored as "feeding" if they resulted in the retention of
1135 particles in the anterior pharynx (arrows), while pumps were scored as "spitting" if they
1136 released beads from the procorpus into the environment or if beads ingested during a
1137 procorpus contraction were not retained. In feeding pumps, the metastomal filter was
1138 typically partially closed, such that food accumulated in the buccal cavity (arrowheads
1139 and inset). Spitting pumps involved the opening of the metastomal filter such that the
1140 buccal cavity did not fill.

1141 (D) Raster plot of representative results from polystyrene bead feeding assay. Animals
1142 carried the transgene *nIs678 ($M1_{promoter}$::gcamp6s)*. "$M1_{promoter}$" refers to the *glr-2*
1143 promoter.

1144 (E) Quantification of average grinder pumping and spitting rates of animals shown in
1145 (D).

1146 (F) Representative images of the pumping cycles of feeding (left column) and spitting
1147 worms (right column). When open, the lumen of the pharynx (arrowheads) is visible as a
1148 white line. The food-trapping pharyngeal valve (left arrowhead) is located at the anterior
1149 end of the lumen. In the absence of UV light (left column), the lumen and pharyngeal
1150 valve open (yellow arrowheads) and close (white arrowheads) nearly synchronously,
1151 enabling the trapping and eventual ingestion of food (Fang-yen *et al.*, 2009). By
1152 contrast, in the presence of UV (right column) light the opening of the lumen and the
1153 pharyngeal valve become uncoupled. While the lumen continues to open and close, the
1154 muscle region at the site of the pharyngeal valve undergoes sustained contraction and
1155 thus opens the valve such that the conclusion of a pump ejects material from the
1156 pharynx. Animals were *unc-29(e1072)* mutants to facilitate video capture.
1157 (G) Quantification of frequencies at which the metastomal filter was open in feeding and
1158 spitting pumps in (D). Center bar, mean; error bars, standard deviation (SD). ****, $p <$
1159 $0.0001$; t test.
1160 (H) Diagrammatic summary of feeding and spitting behavior.
1161 Shading around traces indicates standard error of the mean (SEM). See also **Figure**
1162 **supplement 1**.

1163 **Figure 2. Subcellularly Localized Muscle Contractions and Calcium Increases**

1164 **Open the Pharyngeal Valve to Produce Spitting**

1165 (A) Anatomy of the anterior pharynx showing pharyngeal muscles pm1, pm2, and pm3.

1166 Double-headed arrows indicate orientation of muscle fibers.

1167 (B-E) Mock-ablated (n = 9 animals), pm1-ablated (n = 5), pm2-ablated (n = 8), and

1168 pm1/pm2 double-ablated animals (n = 4) are wild-type in light-induced spitting. All

1169 animals carried transgene *nIs507 (pm1$_{promoter}$::gfp)* to mark pm1. *"pm1$_{promoter}$"* refers to

1170 the *inx-4* promoter.

1171 (F) Diagram of the eight classes of pharyngeal muscle (pm1-8; borders indicated by thin

1172 solid black lines; lumen indicated with thick solid black lines). Dashed boxes indicate

1173 regions analyzed for GCaMP3 fluorescence changes.

1174 (G) Representative images from video of pharyngeal muscle GCaMP3 calcium imaging.

1175 Yellow arrowhead indicates spatially restricted calcium increases. Images false-colored

1176 based on the intensity of fluorescence changes. See also Video 6.

1177 (H) Light induces increases in pharyngeal muscle calcium. Regions analyzed are

1178 indicated in (F). n = 13 animals.

1179 (I) Spatially restricted calcium increases occur even when light does not induce pumps.

1180 Regions adjacent to the anterior tip of the pharynx do not exhibit sustained calcium

1181 signals when the pharynx is not pumping. Regions analyzed are indicated in (F). n = 9

1182 animals.

1183 (J) Laser ablation of the pm2 pharyngeal muscles partially suppresses the light-induced
1184 opening of the metastomal filter. Center bar, mean; error bars, SD. ***, $p < 0.001$; t test.
1185 $n \geq 5$ animals.
1186 Shading around traces indicates SEM. Animals in (G-J) carried transgene *nIs686*
1187 *(pharyngeal muscle$_{promoter}$::gcamp3). "pharyngeal muscle$_{promoter}$"* refers to the *gpa-16*
1188 promoter. See also **Figure supplement 1**.

1189 **Figure 3. Pharyngeally-Expressed Gustatory Receptor Orthologs *lite-1* and *gur-3***

1190 **Play Major and Minor Roles, Respectively, in the Light-Induced Spitting Reflex**

1191 (A) *gur-3* is not required for light-induced burst pumping. n = 3 biological replicates (60

1192 animals total).

1193 (B-C) The contribution of *lite-1* to burst pumping cannot be evaluated directly because

1194 *lite-1* mutants are partially defective in pumping inhibition. $n_{lite\text{-}1}$ = 2 biological replicates

1195 (40 animals total); $n_{lite\text{-}1\ gur\text{-}3}$ = 20 animals.

1196 (D-F) Burst pumping of *eat-2(ad1113)* mutants depends on *lite-1* but not *gur-3*. n = 3

1197 biological replicates (60 animals total).

1198 (G) *lite-1* rescuing transgene *nIs687* (*lite-1*$_{promoter}$*::gfp::lite-1)* rescues the burst pumping

1199 defect of *eat-2; lite-1 gur-3* mutants. n = 3 biological replicates (60 animals total).

1200 (H-K) Light-induced spitting is reduced in *gur-3* and *lite-1* single mutants and eliminated

1201 in *lite-1 gur-3* double mutants. n = 10 animals except $n_{gur\text{-}3}$ = 9.

1202 (L-M) Expression of wild-type *lite-1 (*transgene *nEx2281; lite-1*$_{promoter}$*::lite-1::gfp)* or *gur-3*

1203 (transgene *nEx2157*; *gur-3*$_{promoter}$*::gur-3 gDNA*) respectively restores wild-type or partial

1204 spitting to *lite-1 gur-3* double mutants. n = 10 animals.

1205 (N) Quantification of average spitting rate during light exposure of animals from (H-M).

1206 (O) Quantification of the frequencies at which the metastomal filter was open in feeding

1207 and spitting pumps in (H-M).

1208 (P-R) Light-induced pharyngeal muscle calcium increases depend on *lite-1* (which
1209 accounts for 99% of the response) and *gur-3* (which makes a small contribution to the
1210 initial activation of pharyngeal muscle; black arrows). n ≥ 20 animals.
1211 Shading around traces indicates SEM. All *gur-3* alleles are null allele *gur-3*(*ok2245)* and
1212 all *lite-1* alleles are null allele *lite-1*(*ce314)*. Center bar, mean; error bars, SD. ****, $p < 0.0001$; ***, $p < 0.0005$, **, $p < 0.005$; n.s., not significant; ordinary one-way ANOVA.
1214 See also **Figure supplement 1**.
1215

1216 **Figure 4. The Pharyngeal Neuron M1 Controls the Spitting Reflex**

1217 (A) The anatomy of M1 (red) suggests that it controls spitting directly, as it is the only
1218 neuron to make neuromuscular junctions (bolded blue segment) with the region of
1219 pharyngeal muscle that undergoes sustained contraction during spitting.
1220 (B-C) M1 laser-ablated, but not mock-ablated, animals are completely defective in light-
1221 induced spitting and burst pumping. Animals carried GFP reporter transgene *nIs864*
1222 *($M1_{promoter}$::gfp)* to mark M1. *"$M1_{promoter}$"* refers to the *glr-2* promoter. n ≥ 12 animals.
1223 (D-E) M1 genetically-ablated animals, but not transgene-negative sibling controls, are
1224 completely defective in light-induced spitting and burst pumping. Ablated animals
1225 carried genetic-ablation transgene *nEx2905* (*$M1_{promoter}$::ice::sl2::mcherry*) and all
1226 animals carried GFP reporter transgene *nIs864.* "*$M1_{promoter}$*" refers to the *lury-1*
1227 promoter. n = 10 animals.
1228 (F) Spatially restricted calcium signals depend on M1. Region analyzed is indicated in
1229 Figure 2F. n ≥ 11 animals. Animals carried pharyngeal muscle GCaMP3 transgene
1230 *nIs686*.
1231 (G) Representative example of light-induced GCaMP6s fluorescence increase in M1.
1232 Animals carried transgene *nIs678 ($M1_{promoter}$::gcamp6s)*. "*$M1_{promoter}$"* refers to the *glr-2*
1233 promoter. The unchanging signal common to both images was caused by GCaMP6s
1234 fluorescence in additional *glr-2*-expressing neurons in the nerve ring. See also Video 8.
1235 (H) Heatmap of light-induced GCaMP6s fluorescence increases ($F/F_0$) in the M1 soma.
1236 Each row is a different animal; n = 20.

1237 (I) Average response of animals shown in (H).

1238 (J-L) Light-induced calcium increases in the M1 neuron depend on *lite-1* (which
1239 accounts for 99% M1's response) and *gur-3 (*which makes a small but consistent
1240 contribution to M1's initial activation; black arrows). n = 3 biological replicates (more
1241 than 60 animals total).

1242 (M) Light-induced calcium increases in M1 are reduced but still significant in *unc-*
1243 *13(s69)* mutants. n = 2 biological replicates (greater than 41 animals total).

1244 (N) Quantification of M1's calcium response to light in *unc-13(s69)* mutants in (M). Error
1245 bars, SEM; *, $p < 0.05$; t test.

1246 (O) Light-induced calcium increases in M1 are reduced but still significant in *unc-*
1247 *31(u280)* mutants. n = 20 animals.

1248 (P) Quantification of M1's calcium response to light in *unc-31(u280)* mutants in (O).
1249 Error bars, SEM; **, $p < 0.01$; t test.

1250 (Q-R) A subset (~25%) of *lite-1 gur-3* animals expressing an M1-specific ChR2
1251 transgene *nEx2815 (*$M1_{promoter}$*::chr2::sl2::mcherry)* grown in the presence, but not the
1252 absence, of ATR spit in response to 470 nm light. "$M1_{promoter}$" refers to the *lury-1*
1253 promoter. n ≥ 10 animals.

1254 Shading around traces indicates SEM. All *gur-3* alleles are null allele *gur-3*(*ok2245),*
1255 and all *lite-1* alleles are null allele *lite-1*(*ce314)*. See also **Figure supplement 1** and
1256 **Figure supplement 2**.

1257 **Figure 5. The *gur-3*-Expressing I2 Neurons Can Activate M1 to Produce an**

1258 **Attenuated Form of Spitting**

1259 (A-B) I2-specific expression of *gur-3* restores light-induced spitting to *lite-1 gur-3*

1260 mutants. n = 5 animals.

1261 (C) Quantification of the frequencies at which the metastomal filter was open in feeding

1262 and spitting pumps in (A) and (B). Center bar, mean; error bars, SEM; ****, $p < 0.0001$; t

1263 test. n = 5 animals.

1264 (D) I2-specific expression of *gur-3* restores the light-induced M1 calcium response of

1265 *lite-1 gur-3* mutants. n ≥ 26 animals.

1266 (E-F) Laser ablation of M1 suppresses the I2-specific *gur-3* rescue of *lite-1 gur-3* spitting

1267 defects. n = 11 animals.

1268 (G) Quantification of the frequencies at which the metastomal filter was open in feeding

1269 and spitting pumps in (E) and (F). Center bar, mean; error bars, SEM; ****, $p < 0.0001$; t

1270 test. n ≥ 8 animals.

1271 (H) I2-specific expression of *gur-3* via transgene *nIs791* ($I2_{promoter}$*::mcherry::gur-3(+))*

1272 does not rescue the burst pumping defect of *eat-2; lite-1 gur-3* animals in the grinder

1273 pumping assay. n = 20 animals.

1274 (I) Comparison of grinder pumping rates in (E) and (F). While mock-ablated animals

1275 from (E) do not inhibit pumping in response to light, M1-ablated animals from (F) exhibit

1276 robust light-induced inhibition, indicating that the I2s' promotion of pumping via M1

1277 outweighs their inhibition of pumping.

1278 (J) Comparison of feeding pumping rates from (E) and (F).

1279 (K) Model for the effects of the I2 neurons on M1 and pumping. The I2 neurons reduce
1280 overall feeding by two mechanisms: direct inhibition of feeding pumps and M1-
1281 dependent promotion of spitting pumps.

1282 (L) Genetic ablation of the I2 neurons in a wild-type background does not eliminate light-
1283 induced spitting. n = 5 animals.

1284 (M) Genetic ablation of the I2 neurons of *lite-1(ce314)* mutants does not eliminate light-
1285 induced spitting. n = 6 animals.

1286 Shading around traces indicates SEM. Unless indicated otherwise, "I2-specific
1287 expression of *gur-3"* refers to transgene *nEx2144* ($I2_{promoter}$*::mcherry::gur-3(+))*. "Genetic
1288 ablation of the I2 neurons" refers to transgene *nIs569* ($I2_{promoter}$*::csp-1b)* (Bhatla and
1289 Horvitz, 2015). "$I2_{promoter}$" refers to the *flp-15* promoter.

1290 **Figure 6. The I4 Neuron Functions with the I2 Neurons to Promote Spitting and**
1291 **Inhibit Feeding**

1292 (A) Diagram indicating the cellular morphology of M1 and the *gur-3*-expressing I2 and I4
1293 pharyngeal neurons. The I2 neurons are bilaterally symmetric; only one I2 neuron is
1294 depicted.
1295 (B) Mock-ablated *lite-1* animals inhibit pumping and spit in response to light. n = 8
1296 animals.
1297 (C) I2-ablated *lite-1* animals spit in response to light but do not inhibit pumping. n = 8
1298 animals.
1299 (D) I4-ablated *lite-1* animals inhibit pumping and spit in response to light. n = 10
1300 animals.
1301 (E) I2/I4 double-ablated *lite-1* animals exhibit delayed spitting and do not inhibit
1302 pumping in response to light. n = 8 animals.
1303 (F) Quantification of average spitting rate during light exposure of animals from (B-E).
1304 (G) I2- and I4-ablated *lite-1* animals exhibit small M1 calcium responses; I2/I4 double-
1305 ablated animals do not have detectable M1 calcium responses. n ≥ 8 animals.
1306 (H) Quantification of the frequencies at which the metastomal filter was open in feeding
1307 and spitting pumps in (B-E). n ≥ 4 animals.
1308 (I) Mock-ablated *lite-1* animals inhibit pumping and spit in response to light. n = 5
1309 animals.

1310 (J-L) M1-ablated (n = 6 animals), M1/I2-ablated (n = 6), and M1/I4-ablated (n = 7) *lite-1*

1311 animals inhibit pumping, but do not spit, in response to light.

1312 (M) M1/I2/I4 triple-ablated *lite-1* animals neither inhibit pumping nor spit in response to

1313 light. n = 4 animals.

1314 (N) Quantification of pumping inhibition in (I-M). Ablation of the I2 neurons eliminates

1315 light-induced pumping inhibition.

1316 Shading around traces indicates SEM. All animals were *lite-1*(ce314) null mutants and

1317 carried transgene *nIs678 ($M1_{promoter}$::gcamp6s)*. "$M1_{promoter}$" refers to the *glr-2* promoter.

1318 Center bar, mean; error bars, SD. **, $p < 0.005$; *, $p < 0.05$; n.s., not significant; ordinary

1319 one-way ANOVA.

1320 **Figure 7. Models of Spitting Behavior and Neural Circuitry**

1321 (A) Model for feeding and spitting. During feeding, the M1 neuron is inactive. Thus, the
1322 metastomal filter is partially closed, restricting particle influx, and the pharyngeal valve
1323 closes at the end of each pump, trapping food. During spitting induced by light or
1324 reactive oxygen species (ROS), M1 is active, thus inducing spitting of ingested material
1325 by opening the pharyngeal valve and facilitating rinsing of the pharynx by opening the
1326 metastomal filter.

1327 (B) Model for neural circuitry controlling light- and ROS-induced spitting. Light or ROS
1328 stimulate the M1, I2, and I4 neurons via LITE-1 and GUR-3. The I2 and I4 neurons
1329 excite M1, which is situated in the “waist” of an “hourglass” circuit motif. In turn, M1
1330 makes diverging outputs to multiple pharyngeal muscle classes, each driving distinct
1331 aspects of the spitting reflex: the pm1 and pm2 muscles open the metastomal filter, a
1332 subcellular compartment of the pm3 muscles opens the pharyngeal valve, and the
1333 remainder of pm3 pumps. The M1 and I2 neurons each also inhibit pumping.

1334 **Figure 1—figure supplement 1.**

1335 (A) The odor of 9M hydrogen peroxide induces spitting. Animals are *unc-29(e1072)*

1336 mutants to facilitate video capture. n = 4 animals.

1337 (B) Raster plot showing occurrence of “closed” (black) and “open” (green) pumps in

1338 pharyngeal muscle motion visualization assay. n = 7 animals.

1339 (C) Moving averages of animals from (B), indicating that the burst pumping phase

1340 consists almost completely of “open” pumps.

1341 Shading around traces indicates SEM.

1342 **Figure 2—figure supplement 1.**

1343 (A) Quantification of pumps induced by 485 nm light in 10 seconds in immobilized
1344 pumping assay. Laser ablation of M1, but not other pharyngeal neurons, eliminates
1345 light-induced pumping.

1346 (B-C) pm1-ablated animals lack the metastomal filter and thus ingest more material into
1347 the procorpus than mock-ablated controls do. Dark material in the pharyngeal lumen is
1348 a mixture of *E. coli* and 1 µm polystyrene beads. In mock-ablated animals, accumulation
1349 is visible in the pharyngeal isthmus but is minimal in the procorpus of most animals.
1350 pm1-ablated animals accumulate markedly more material in the procorpus. We also
1351 noticed qualitatively that pm1-ablated animals often spit material less efficiently than
1352 control animals, but this difference could stem from the differences in the average
1353 amount of ingested material in the pharynx in each condition. All animals carry
1354 transgene *nIs507* ($pm1_{promoter}$*::gfp).* "$pm1_{promoter}$" refers to the *inx-4* promoter.

1355 **Figure 3—figure supplement 1.**

1356 (A) *egl-47/gur-1(n1082dm)* mutants were normal in burst pumping. n = 20 animals.

1357 (B) *egl-47/gur-1(ok677)* mutants were normal in burst pumping. n = 20 animals.

1358 (C) *gur-4(ok672)* mutants were normal in burst pumping. n = 20 animals.

1359 (D) *gur-5(tm6169)* mutants were normal in burst pumping. n = 20 animals.

1360 (E-F) Integrated *gur-3* transcriptional reporter transgene *nIs780 (gur-3*$_{promoter}$*::gfp)* is

1361 expressed in the MI and M1 pharyngeal neurons and an unidentified head neuron (not

1362 shown), in addition to being expressed in the I2, I4, and AVD neurons as previously

1363 reported by Bhatla and Horvitz (2015).

1364 Shading around traces indicates SEM.

1365 **Figure 4—figure supplement 1.**

1366 (A) Overexpression of the mammalian caspase ICE in M1 via the transgene *nEx2905*
1367 (*M1*$_{promoter\ –\ lury\text{-}1}$*::ice::sl2::mCherry)* kills M1 with high efficiency and the M2 pharyngeal
1368 neurons with moderate efficiency. The presence of M1 and the M2s was determined by
1369 the expression of transgenes *nIs864 (M1*$_{promoter\ –\ glr\text{-}2}$*::gfp)* and *nIs310 (nlp-13*$_{promoter}$*::gfp)*,
1370 respectively.

1371 (B) M1 genetic-ablation transgene eliminates burst pumping in the grinder pumping
1372 assay. Ablation animals carried transgene *nEx2905 (M1*$_{promoter\ -\ lury\text{-}1}$*::ice::sl2::mcherry);*
1373 all animals carried *nIs864 (M1*$_{promoter\ –\ glr\text{-}2}$*::gfp).* n = 40 animals.

1374 (C) Screening animals based on the brightness of pharyngeal mCherry expression
1375 allows the selection of animals lacking the M1 neuron but not the M2 neurons. When
1376 pharyngeal muscle mCherry expression is high, animals are more likely to lack the M2s.
1377 Animals with dim pharyngeal muscle mCherry expression very rarely lack M2s; thus dim
1378 mCherry expression can be used to enrich for animals lacking only M1. Center bar,
1379 mean; error bars, SEM. n = 3 biological replicates (more than 65 animals total).

1380 (D) Genetic ablation of M1 eliminates burst pumping in *eat-2* mutants. Ablation animals
1381 carried transgene *nIs865* (*M1*$_{promoter\ –\ lury\text{-}1}$*::ice::sl2::mCherry).* n = 3 biological replicates
1382 (60 animals total).

1383 (E) Comparison of grinder pumping rates of mock- and M1-ablated animals from Figure
1384 4B and 4C. In addition to eliminating burst pumping and spitting, M1 ablation enhances
1385 the rate of pumping recovery after illumination. n ≥ 12 animals.

1386 (F) Laser-ablated animals from Figure 4B exhibit abnormal “uncoupled” pumps, during
1387 which the grinder pumps while the procorpus does not. n ≥ 12 animals.
1388 (G) Comparison of grinder pumping rates of control and M1-ablated animals from Figure
1389 4D and 4E. In addition to eliminating burst pumping and spitting, M1 ablation enhances
1390 the rate of pumping recovery after illumination. n = 10 animals.
1391 (H) M1 genetic-ablation animals from Figure 4E exhibit abnormal “uncoupled” pumps,
1392 during which the grinder pumps while the procorpus does not. n = 10 animals.
1393 (I) *unc-17(e245)* vesicular acetylcholine transporter mutants defective in vesicular
1394 acetylcholine transport were severely defective in both feeding and burst pumping. n = 3
1395 biological replicates (60 animals total).
1396 (J) *cha-1(p1152)* choline acetyltransferase mutants defective in acetylcholine synthesis
1397 were severely defective in both feeding and burst pumping. n = 20 animals.
1398 (K) *ric-3(md158)* mutants defective in nicotinic acetylcholine receptor maturation were
1399 severely defective in both feeding and burst pumping. n = 20 animals.
1400 (L) *unc-25(e156)* glutamate decarboxylase mutants defective in GABA synthesis were
1401 normal in burst pumping. n = 20 animals.
1402 (M) *eat-4(ky5)* vesicular glutamate transporter mutants defective in vesicular glutamate
1403 transport were defective in acute inhibition (Bhatla and Horvitz, 2015) but normal in
1404 burst pumping. n = 20 animals.
1405 (N) *cat-2(e1113)* tyrosine hydroxylase mutants defective in dopamine synthesis were
1406 normal in burst pumping. n = 20 animals.

1407 (O) *tdc-1(n3420)* tyrosine decarboxylase mutants defective in tyramine and octopamine
1408 synthesis were normal in burst pumping. n = 20 animals.
1409 (P) *tph-1(n4622)* tryptophan hydroxylase mutants defective in serotonin synthesis were
1410 mildly defective in both feeding and burst pumping. n = 3 biological replicates (60
1411 animals total).
1412 (Q) *tph-1(mg280)* tryptophan hydroxylase mutants defective in serotonin synthesis were
1413 mildly defective in both feeding and burst pumping. n = 3 biological replicates (60
1414 animals total).
1415 (R) *ser-4(ok512); mod-1(ok103); ser-1(ok345) ser-7(tm1325)* quadruple serotonin
1416 receptor mutants were defective in feeding but normal in burst pumping. n = 20 animals.
1417 Shading around traces indicates SEM. "$M1_{promoter-lury-1}$" refers to the *lury-1* promoter
1418 and "$M1_{promoter-glr-2}$" refers to the *glr-2* promoter. Panels (E-H) are derived from videos
1419 of bead feeding assays, all other behavior plots were grinder pumping assays scored in
1420 real time.

1421 **Figure 4—figure supplement 2: Burst pumping responses of acetylcholine**
1422 **receptor mutants to UV light.**

1423 (A) *lev-1/acr-1(e211)* nicotinic acetylcholine receptor mutants were normal in burst
1424 pumping. n = 20 animals.
1425 (B) *acr-2(n2595 n2420)* nicotinic acetylcholine receptor mutants were normal in burst
1426 pumping. n = 20 animals.
1427 (C) *acr-3(ok2049)* nicotinic acetylcholine receptor mutants were normal in burst
1428 pumping. n = 20 animals.
1429 (D) *deg-3(u662); des-2/acr-4(u695)* nicotinic acetylcholine receptor mutants were
1430 normal in burst pumping. n = 20 animals.
1431 (E) *acr-5(ok180)* nicotinic acetylcholine receptor mutants were normal in burst pumping.
1432 n = 20 animals.
1433 (F) *acr-6(tm3723)* nicotinic acetylcholine receptor mutants were subtly defective in burst
1434 pumping. n = 3 biological replicates (60 animals total).
1435 (G) *acr-7(tm863)* nicotinic acetylcholine receptor mutants were modestly defective in
1436 burst pumping. n = 3 biological replicates (60 animals total).
1437 (H) *acr-8(ok1240)* nicotinic acetylcholine receptor mutants were normal in burst
1438 pumping. n = 3 biological replicates (60 animals total).
1439 (I) *acr-10(tm2515)* nicotinic acetylcholine receptor mutants were normal in burst
1440 pumping. n = 20 animals.

1441 (J) *acr-11(gk827759)* nicotinic acetylcholine receptor mutants were normal in burst
1442 pumping. n = 20 animals.
1443 (K) *acr-12(ok367)* nicotinic acetylcholine receptor mutants were normal in burst
1444 pumping. n = 20 animals.
1445 (L) *lev-8/acr-13(x15)* nicotinic acetylcholine receptor mutants were normal in burst
1446 pumping. n = 20 animals.
1447 (M) *acr-14(tm5819)* nicotinic acetylcholine receptor mutants were normal in burst
1448 pumping. n = 20 animals.
1449 (N) *acr-15(ok1214)* nicotinic acetylcholine receptor mutants were normal in burst
1450 pumping. n = 20 animals.
1451 (O) *acr-16(ok789)* nicotinic acetylcholine receptor mutants were normal in burst
1452 pumping. n = 20 animals.
1453 (P) *acr-17(gk804825)* nicotinic acetylcholine receptor mutants were defective in both
1454 feeding and burst pumping. n = 2 biological replicates (40 animals total).
1455 (Q) *acr-17(gk661490)* nicotinic acetylcholine receptor mutants were normal in burst
1456 pumping. n = 20 animals.
1457 (R) *acr-18(gk324494)* nicotinic acetylcholine receptor mutants were defective in feeding
1458 but normal in burst pumping. n = 20 animals.
1459 (S) *acr-19(ok967)* nicotinic acetylcholine receptor mutants were normal in burst
1460 pumping. n = 20 animals.

1461 (T) *acr-20(gk161737)* nicotinic acetylcholine receptor mutants were normal in burst
1462 pumping. n = 20 animals.
1463 (U) *acr-21(ok1314)* nicotinic acetylcholine receptor mutants were normal in burst
1464 pumping. n = 20 animals.
1465 (V) *acr-23(gk231233)* nicotinic acetylcholine receptor mutants were subtly defective in
1466 feeding and defective in burst pumping. n = 3 biological replicates (60 animals total).
1467 (W) *acr-23(ox429)* nicotinic acetylcholine receptor mutants were subtly defective in
1468 burst pumping. n = 3 biological replicates (60 animals total).
1469 (X) *acr-23(ok2804)* nicotinic acetylcholine receptor mutants were normal in burst
1470 pumping. n = 20 animals.
1471 (Y) *acr-24(gk387895)* nicotinic acetylcholine receptor mutants were defective in both
1472 feeding and burst pumping. n = 2 biological replicates (40 animals total).
1473 (Z) *acr-24(gk557791)* nicotinic acetylcholine receptor mutants were defective in burst
1474 pumping. n = 3 biological replicates (60 animals total).
1475 (A') *deg-3(u773)* nicotinic acetylcholine receptor mutants were normal in burst pumping.
1476 n = 20 animals.
1477 (B') *unc-29(e1072)* nicotinic acetylcholine receptor mutants were normal in burst
1478 pumping. n = 3 biological replicates (60 animals total).
1479 (C') *unc-38(e264)* nicotinic acetylcholine receptor mutants were normal in burst
1480 pumping. n = 20 animals.

1481 (D') *lev-7/unc-63(x13)* nicotinic acetylcholine receptor mutants were normal in burst
1482 pumping. n = 20 animals.
1483 (E') *acc-1(tm3268)* acetylcholine-gated chloride channel mutants were normal in burst
1484 pumping. n = 20 animals.
1485 (F') *acc-2(gk501637)* acetylcholine-gated chloride channel mutants were normal in burst
1486 pumping. n = 20 animals.
1487 (G') *acc-2(ok2216)* acetylcholine-gated chloride channel mutants were defective in
1488 feeding and burst pumping. n = 3 biological replicates (60 animals total).
1489 (H') *acc-2(tm3219)* acetylcholine-gated chloride channel mutants were normal in burst
1490 pumping. n = 20 animals.
1491 (I') *acc-3(tm3174)* acetylcholine-gated chloride channel mutants were normal in burst
1492 pumping. n = 20 animals.
1493 (J') *acc-4(ok2371)* acetylcholine-gated chloride channel mutants were normal in burst
1494 pumping. n = 20 animals.
1495 (K') *lgc-40(tm3377)* acetylcholine-gated chloride channel mutants were normal in burst
1496 pumping. n = 20 animals.
1497 (L') *pbo-5(gk963058)* nicotinic acetylcholine receptor family mutants were normal in
1498 burst pumping. n = 20 animals.
1499 (M') *pbo-6(ok1564)* nicotinic acetylcholine receptor family mutants were normal in burst
1500 pumping. n = 20 animals.

1501 (N’) *gar-1(ok755)* muscarinic acetylcholine receptor mutants were subtly defective in

1502 burst pumping. n = 3 biological replicates (60 animals total).

1503 (O’) *gar-2(ok520)* muscarinic acetylcholine receptor mutants were normal in burst

1504 pumping. n = 20 animals.

1505 (P’) *gar-3(gk337)* muscarinic acetylcholine receptor mutants were normal in burst

1506 pumping. n = 20 animals.

1507 **Video 1: Feeding pumps in polystyrene bead feeding assay.**

1508 High frame rate video of *C. elegans* feeding in polystyrene bead feeding assay. The
1509 small, dark particles are polystyrene beads. During typical feeding pumps, beads
1510 accumulate in the buccal cavity. Beads filter gradually from the buccal cavity into the
1511 pharyngeal lumen, where they are trapped by the closure of the pharyngeal valve at the
1512 front of the pharynx upon the conclusion of each pump. Video was recorded at 1,000
1513 frames per second. Playback is at 3% of original speed.

1514

1515 **Video 2: Spitting pumps in polystyrene bead feeding assay.**

1516 High frame rate video of *C. elegans* spitting in response to light in polystyrene bead
1517 feeding assay. During spitting pumps, beads no longer accumulate in the buccal cavity,
1518 but instead freely enter the pharyngeal lumen. At the end of the pump, all ingested
1519 material is expelled. Video was recorded at 1,000 frames per second. Playback is at 3%
1520 of original speed.

1521

1522 **Video 3: Feeding pumps in muscle motion visualization assay.**

1523 Video of *C. elegans* feeding beneath a coverslip. The pharyngeal lumen is visible as a
1524 white space when it is opened by the contraction of pharyngeal muscle. In feeding, the
1525 musculature of the anterior pharynx relaxes at the end of each pump, closing the
1526 pharyngeal valve and thereby trapping ingested material. Video was recorded at 86
1527 frames per second. Playback is at 50% of original speed.

1528

1529 **Video 4: Spitting pumps in muscle motion visualization assay.**

1530 Video of *C. elegans* beneath a coverslip spitting in response to light. In contrast to
1531 feeding pumps, spitting pumps are characterized by the sustained contraction of the
1532 anterior musculature of the pharynx, which remains contracted open as the rest of the
1533 pharynx continues to contract and relax. Video was recorded at 86 frames per second.
1534 Playback is at 50% of original speed.

1535

1536 **Video 5: "Gulping" pumps in polystyrene bead feeding assay.**

1537 High frame rate video of *C. elegans* "gulping" in polystyrene bead feeding assay.
1538 As in spitting pumps, beads pass freely through the buccal cavity and into the
1539 pharyngeal lumen. As in feeding pumps, this material is subsequently trapped and
1540 retained by the pharyngeal valve, resulting in ingestion. Video was recorded at 1,000
1541 frames per second. Playback is at 3% of original speed.

1542

1543 **Video 6: Pharyngeal muscle calcium response to light.**

1544 The pharyngeal muscle calcium response to light, as reported by GCaMP3
1545 fluorescence. Pumps result in fluorescence increases across the entirety of the anterior
1546 pharynx. Before and between pumps, localized and sustained calcium increases occur
1547 at the anterior tip of the pharynx. Video was recorded at 15 frames per second and

1548 false-colored based on the intensity of fluorescence changes (blue, low intensity; red,
1549 high intensity). Playback is in real time.
1550
1551 **Video 7: pm2-ablated animals are defective in opening the metastomal filter**
1552 **during spitting behavior in polystyrene bead feeding assay.**
1553 High frame rate video of pm2-ablated *C. elegans* spitting in response to light in
1554 polystyrene bead feeding assay. In contrast to typical spitting pumps, beads accumulate
1555 in the buccal cavity, indicating that the metastomal filter is partially closed. At the end of
1556 the pump, ingested material is still expelled, indicating that the pharyngeal valve is
1557 open. Video was recorded at 1,000 frames per second. Playback is at 3% of original
1558 speed.
1559
1560 **Video 8: The pharyngeal neuron M1 is activated by light.**
1561 The pharyngeal neuron M1 is acutely activated by light, as reported by GCaMP6s
1562 fluorescence. Video was recorded at 2 frames per second and false-colored based on
1563 the intensity of fluorescence changes (blue, low intensity; red, high intensity). Playback
1564 is at 100% of original speed.

**Figure 1**

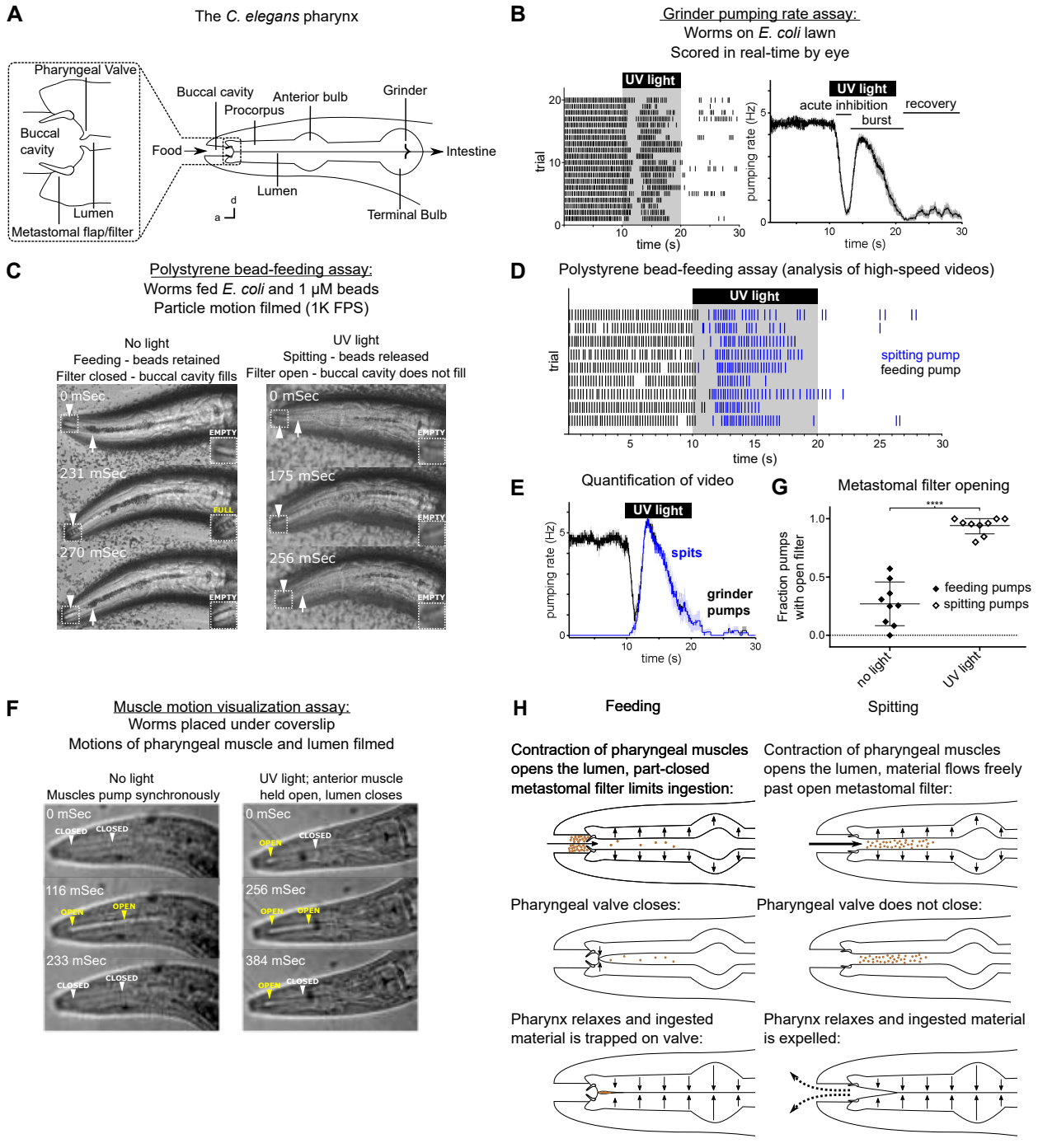
A
The C. elegans pharynx
Pharyngeal Valve
Buccal cavity
Lumen
Metastomal flap/filter
Buccal cavity
Procorpus
Anterior bulb
Grinder
Food
Intestine
Lumen
Terminal Bulb
d
a
B
Grinder pumping rate assay:
Worms on E. coli lawn
Scored in real-time by eye
UV light
trial
time (s)
UV light
acute inhibition
burst
recovery
pumping rate (Hz)
time (s)
C
Polystyrene bead-feeding assay:
Worms fed E. coli and 1 µM beads
Particle motion filmed (1K FPS)
No light
Feeding - beads retained
Filter closed - buccal cavity fills
UV light
Spitting - beads released
Filter open - buccal cavity does not fill
0 mSec
231 mSec
270 mSec
0 mSec
175 mSec
256 mSec
EMPTY
FULL
D
Polystyrene bead-feeding assay (analysis of high-speed videos)
UV light
trial
spitting pump
feeding pump
time (s)
E
Quantification of video
UV light
spits
grinder pumps
pumping rate (Hz)
time (s)
G
Metastomal filter opening
****
Fraction pumps with open filter
feeding pumps
spitting pumps
no light
UV light
F
Muscle motion visualization assay:
Worms placed under coverslip
Motions of pharyngeal muscle and lumen filmed
No light
Muscles pump synchronously
UV light; anterior muscle held open, lumen closes
0 mSec
116 mSec
233 mSec
0 mSec
256 mSec
384 mSec
CLOSED
OPEN
H
Feeding
Spitting
Contraction of pharyngeal muscles opens the lumen, part-closed metastomal filter limits ingestion:
Contraction of pharyngeal muscles opens the lumen, material flows freely past open metastomal filter:
Pharyngeal valve closes:
Pharyngeal valve does not close:
Pharynx relaxes and ingested material is trapped on valve:
Pharynx relaxes and ingested material is expelled:

**Figure 2**

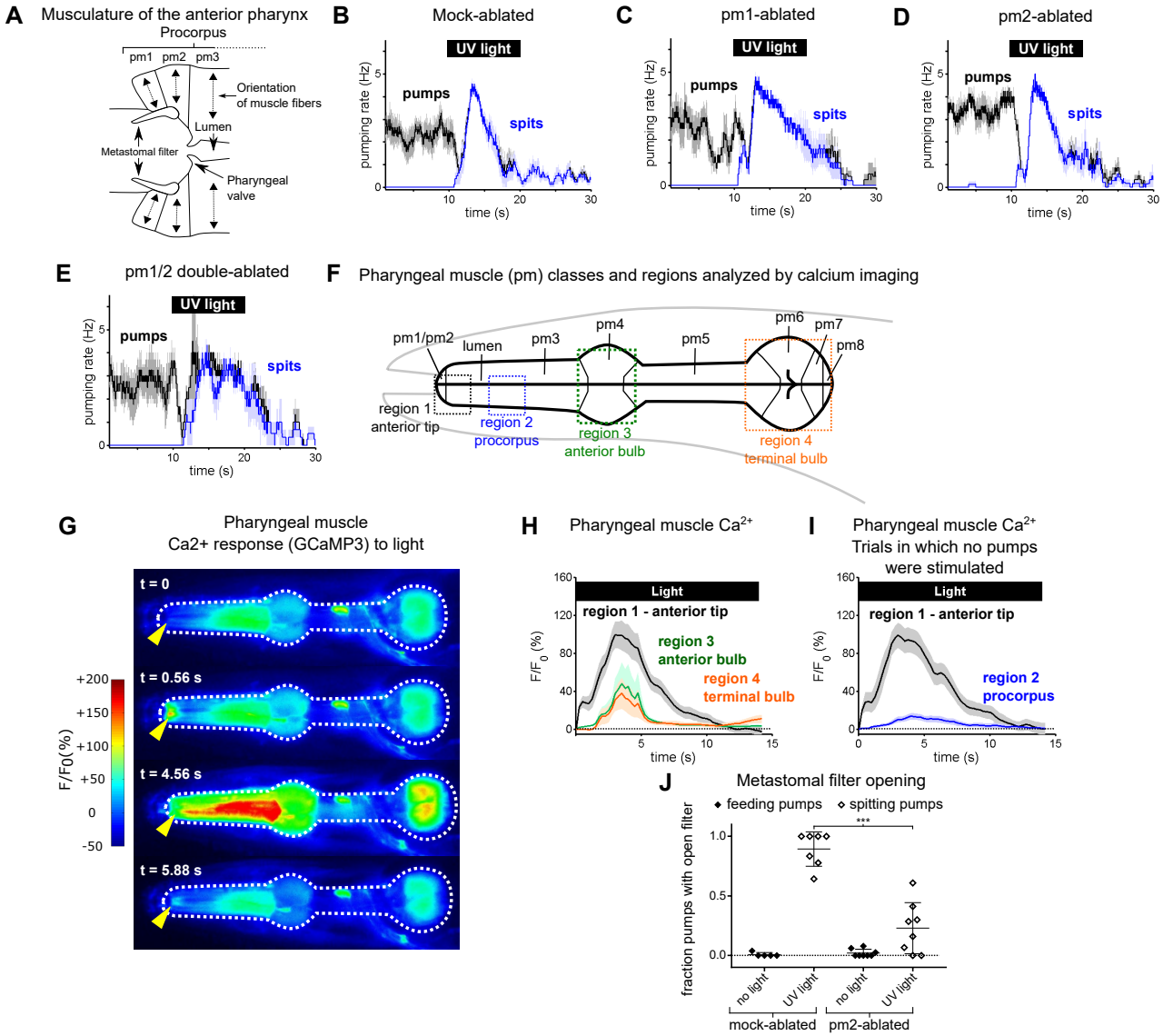
A
Musculature of the anterior pharynx
Procorpus
pm1 pm2 pm3
Orientation of muscle fibers
Lumen
Metastomal filter
Pharyngeal valve
B
Mock-ablated
UV light
pumps
spits
pumping rate (Hz)
time (s)
C
pm1-ablated
D
pm2-ablated
E
pm1/2 double-ablated
F
Pharyngeal muscle (pm) classes and regions analyzed by calcium imaging
pm1/pm2
lumen
pm3
pm4
pm5
pm6
pm7
pm8
region 1
anterior tip
region 2
procorpus
region 3
anterior bulb
region 4
terminal bulb
G
Pharyngeal muscle
Ca2+ response (GCaMP3) to light
t = 0
t = 0.56 s
t = 4.56 s
t = 5.88 s
F/F0(%)
+200
+150
+100
+50
0
-50
H
Pharyngeal muscle Ca2+
Light
region 1 - anterior tip
region 3
anterior bulb
region 4
terminal bulb
F/F0 (%)
time (s)
I
Pharyngeal muscle Ca2+
Trials in which no pumps
were stimulated
region 2
procorpus
J
Metastomal filter opening
feeding pumps
spitting pumps
fraction pumps with open filter
no light
UV light
mock-ablated
pm2-ablated

**Figure 3**

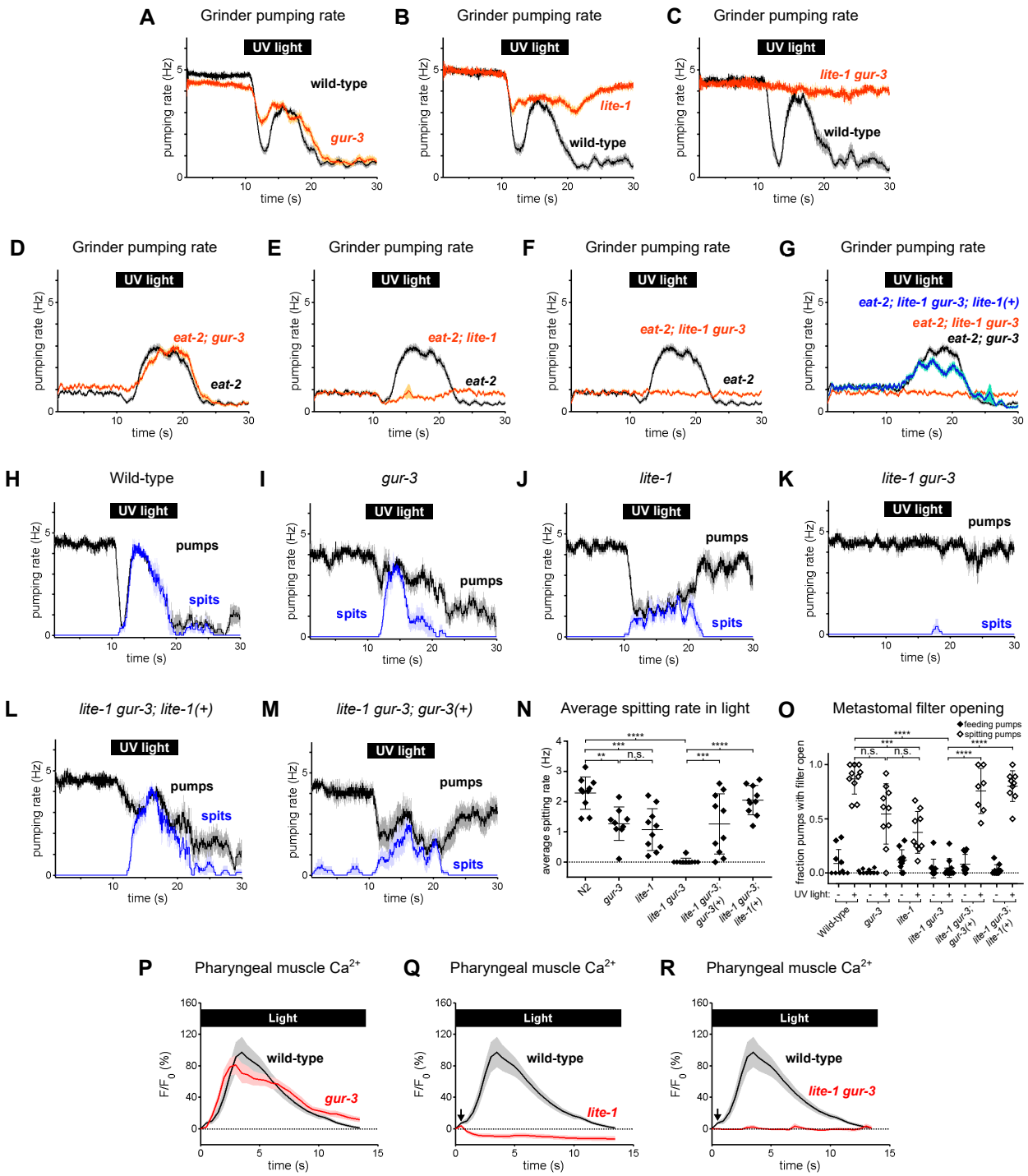
A
Grinder pumping rate
UV light
wild-type
gur-3
pumping rate (Hz)
time (s)
B
Grinder pumping rate
UV light
lite-1
wild-type
C
Grinder pumping rate
UV light
lite-1 gur-3
wild-type
D
Grinder pumping rate
UV light
eat-2; gur-3
eat-2
E
Grinder pumping rate
UV light
eat-2; lite-1
eat-2
F
Grinder pumping rate
UV light
eat-2; lite-1 gur-3
eat-2
G
Grinder pumping rate
UV light
eat-2; lite-1 gur-3; lite-1(+)
eat-2; lite-1 gur-3
eat-2; gur-3
H
Wild-type
UV light
pumps
spits
I
gur-3
UV light
pumps
spits
J
lite-1
UV light
pumps
spits
K
lite-1 gur-3
UV light
pumps
spits
L
lite-1 gur-3; lite-1(+)
UV light
pumps
spits
M
lite-1 gur-3; gur-3(+)
UV light
pumps
spits
N
Average spitting rate in light
average spitting rate (Hz)
N2
gur-3
lite-1
lite-1 gur-3
lite-1 gur-3; gur-3(+)
lite-1 gur-3; lite-1(+)
O
Metastomal filter opening
feeding pumps
spitting pumps
fraction pumps with filter open
UV light:
Wild-type
gur-3
lite-1
lite-1 gur-3
lite-1 gur-3; gur-3(+)
lite-1 gur-3; lite-1(+)
P
Pharyngeal muscle Ca2+
Light
wild-type
gur-3
F/F0 (%)
time (s)
Q
Pharyngeal muscle Ca2+
Light
wild-type
lite-1
R
Pharyngeal muscle Ca2+
Light
wild-type
lite-1 gur-3

**Figure 4**

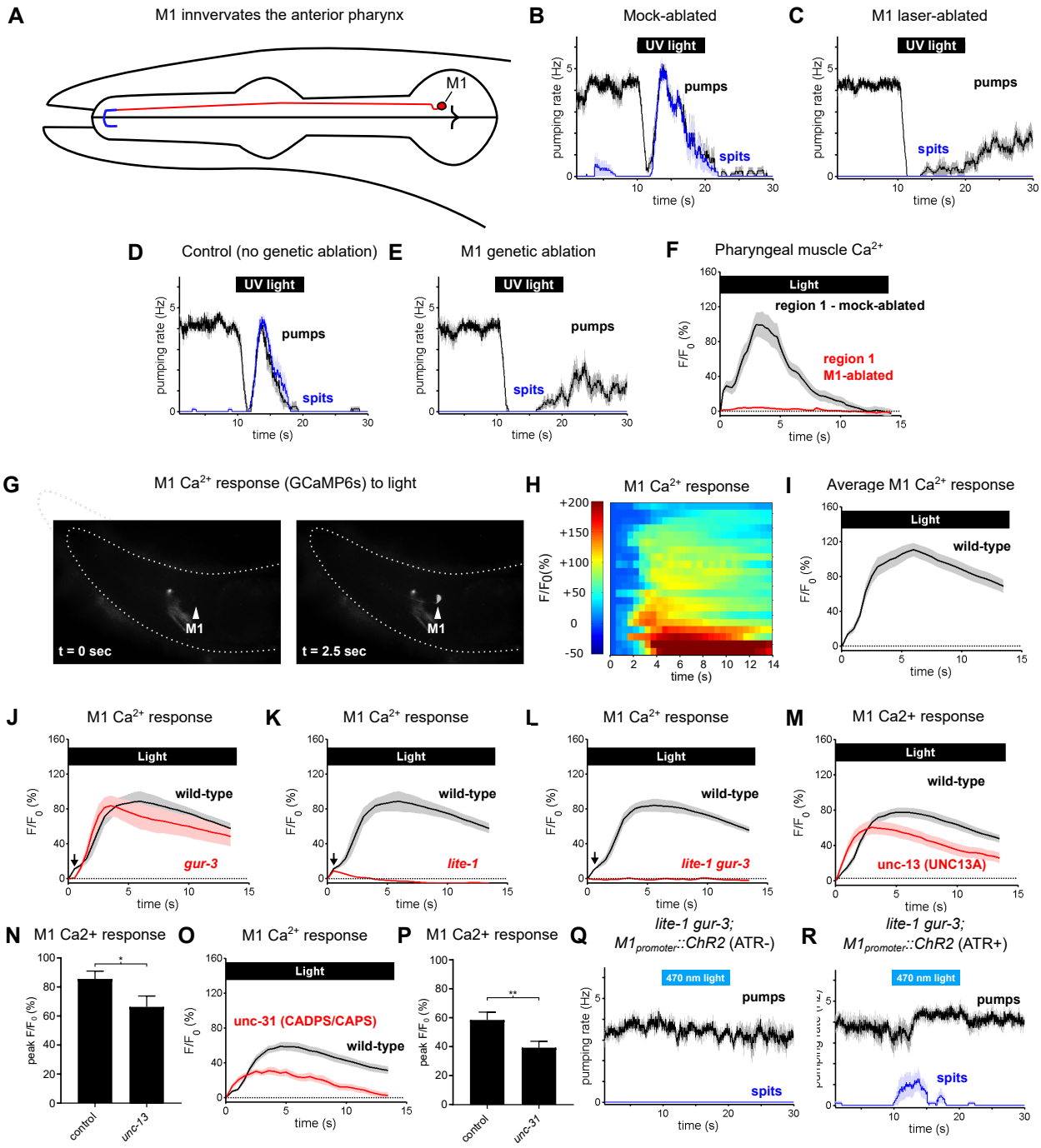
A
M1 innvervates the anterior pharynx
M1
B
Mock-ablated
UV light
pumps
spits
pumping rate (Hz)
time (s)
C
M1 laser-ablated
UV light
pumps
spits
pumping rate (Hz)
time (s)
D
Control (no genetic ablation)
UV light
pumps
spits
pumping rate (Hz)
time (s)
E
M1 genetic ablation
UV light
pumps
spits
pumping rate (Hz)
time (s)
F
Pharyngeal muscle Ca2+
Light
region 1 - mock-ablated
region 1
M1-ablated
F/F0 (%)
time (s)
G
M1 Ca2+ response (GCaMP6s) to light
M1
t = 0 sec
M1
t = 2.5 sec
H
M1 Ca2+ response
F/F0(%)
time (s)
I
Average M1 Ca2+ response
Light
wild-type
F/F0 (%)
time (s)
J
M1 Ca2+ response
Light
wild-type
gur-3
F/F0 (%)
time (s)
K
M1 Ca2+ response
Light
wild-type
lite-1
F/F0 (%)
time (s)
L
M1 Ca2+ response
Light
wild-type
lite-1 gur-3
F/F0 (%)
time (s)
M
M1 Ca2+ response
Light
wild-type
unc-13 (UNC13A)
F/F0 (%)
time (s)
N
M1 Ca2+ response
peak F/F0 (%)
control
unc-13
O
M1 Ca2+ response
Light
unc-31 (CADPS/CAPS)
wild-type
F/F0 (%)
time (s)
P
M1 Ca2+ response
peak F/F0 (%)
control
unc-31
Q
lite-1 gur-3;
M1promoter::ChR2 (ATR-)
470 nm light
pumps
spits
pumping rate (Hz)
time (s)
R
lite-1 gur-3;
M1promoter::ChR2 (ATR+)
470 nm light
pumps
spits
time (s)

**Figure 5**

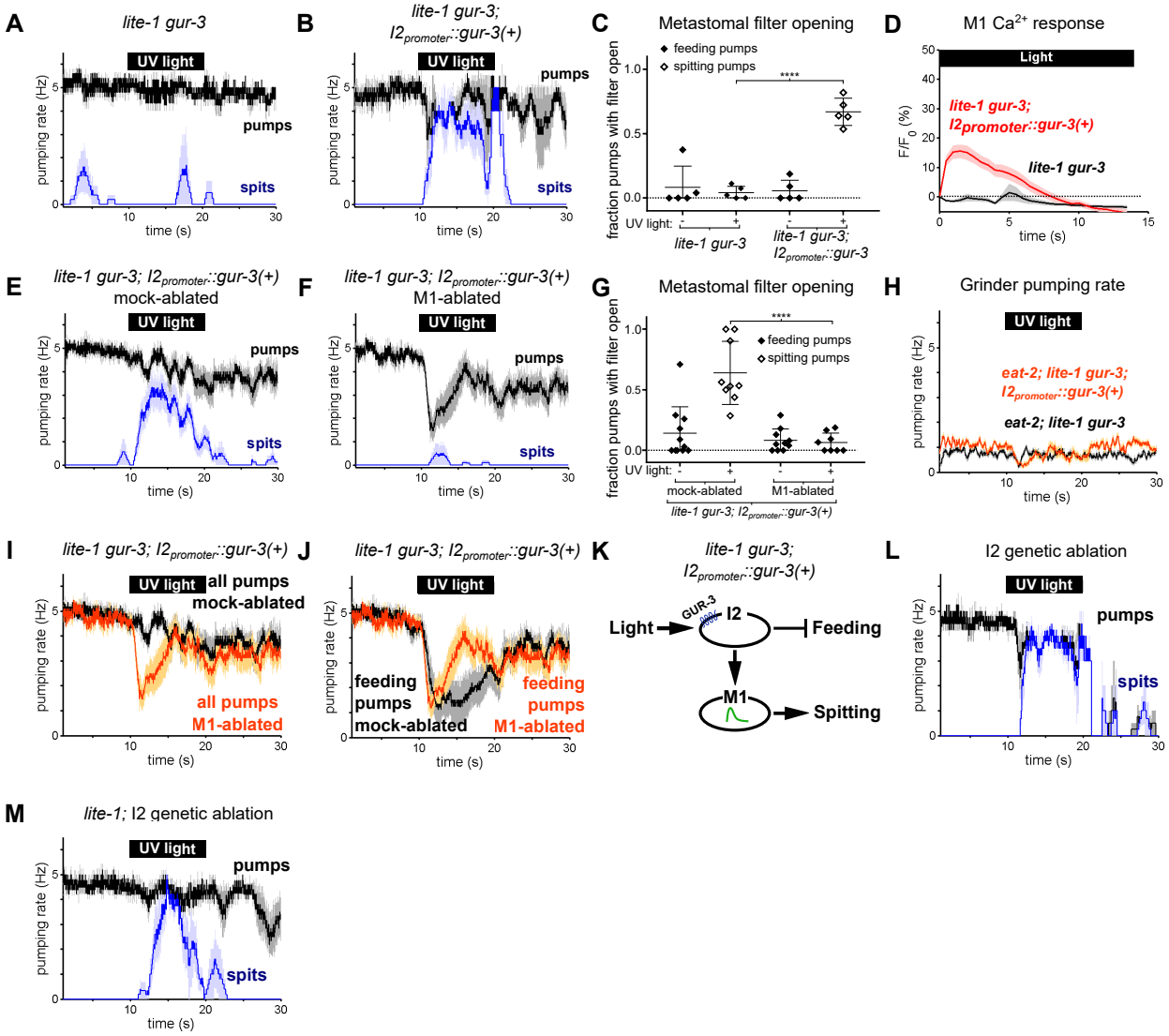
A
lite-1 gur-3
UV light
pumps
spits
pumping rate (Hz)
time (s)
B
lite-1 gur-3; I2promoter::gur-3(+)
UV light
pumps
spits
C
Metastomal filter opening
feeding pumps
spitting pumps
****
fraction pumps with filter open
UV light:
lite-1 gur-3
lite-1 gur-3; I2promoter::gur-3
D
M1 Ca2+ response
Light
lite-1 gur-3; I2promoter::gur-3(+)
lite-1 gur-3
F/F0 (%)
time (s)
E
lite-1 gur-3; I2promoter::gur-3(+)
mock-ablated
UV light
pumps
spits
F
lite-1 gur-3; I2promoter::gur-3(+)
M1-ablated
UV light
pumps
spits
G
Metastomal filter opening
****
feeding pumps
spitting pumps
fraction pumps with filter open
UV light:
mock-ablated
M1-ablated
lite-1 gur-3; I2promoter::gur-3(+)
H
Grinder pumping rate
UV light
eat-2; lite-1 gur-3; I2promoter::gur-3(+)
eat-2; lite-1 gur-3
pumping rate (Hz)
time (s)
I
lite-1 gur-3; I2promoter::gur-3(+)
UV light
all pumps
mock-ablated
all pumps
M1-ablated
J
lite-1 gur-3; I2promoter::gur-3(+)
UV light
feeding pumps
mock-ablated
feeding pumps
M1-ablated
K
lite-1 gur-3; I2promoter::gur-3(+)
Light
GUR-3
I2
Feeding
M1
Spitting
L
I2 genetic ablation
UV light
pumps
spits
M
lite-1; I2 genetic ablation
UV light
pumps
spits

**Figure 6**

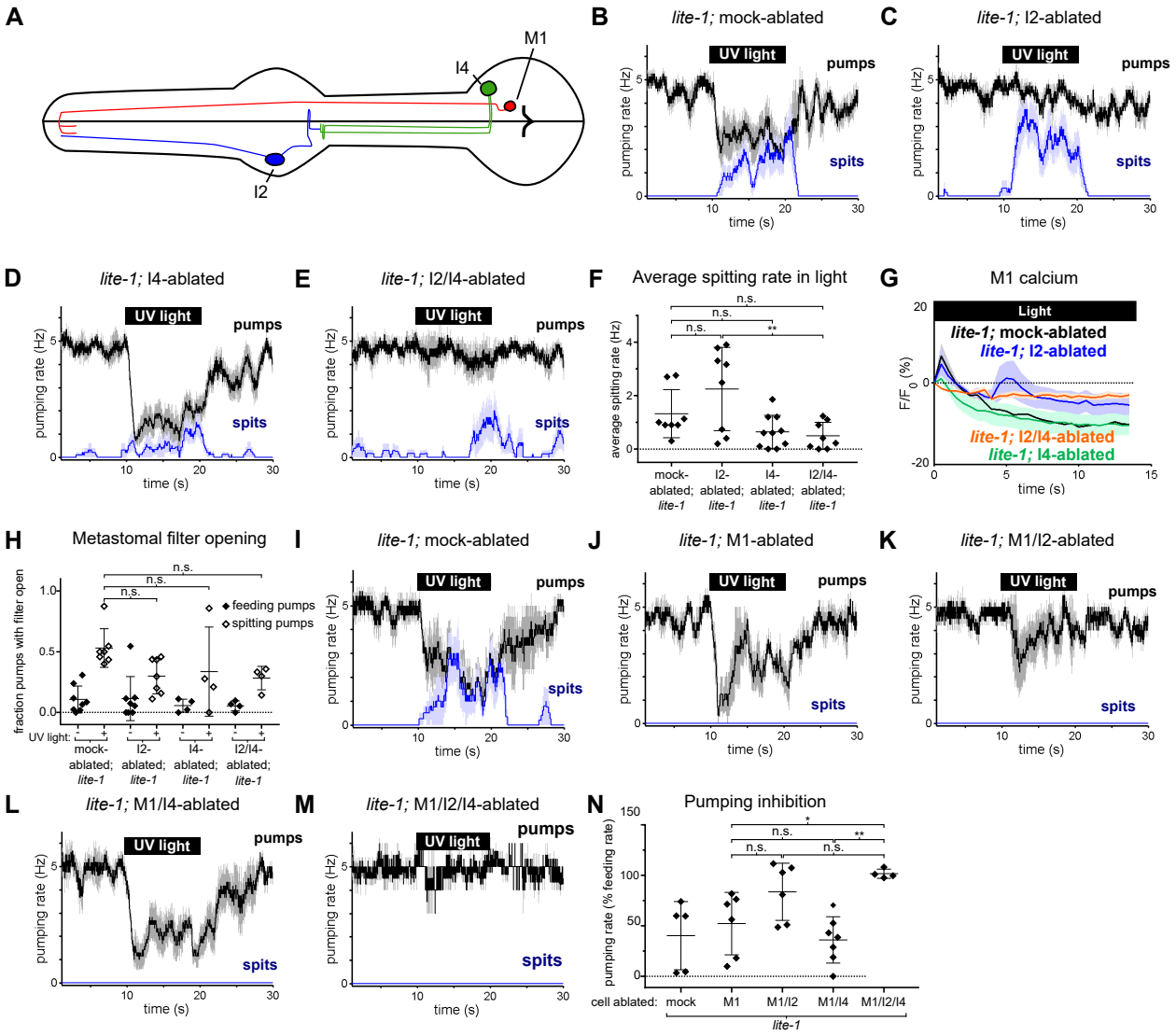
A
M1
I4
I2
B
lite-1; mock-ablated
UV light
pumps
spits
pumping rate (Hz)
time (s)
C
lite-1; I2-ablated
D
lite-1; I4-ablated
E
lite-1; I2/I4-ablated
F
Average spitting rate in light
average spitting rate (Hz)
n.s.
**
mock-ablated; lite-1
I2-ablated; lite-1
I4-ablated; lite-1
I2/I4-ablated; lite-1
G
M1 calcium
Light
lite-1; mock-ablated
lite-1; I2-ablated
lite-1; I2/I4-ablated
lite-1; I4-ablated
F/F0 (%)
H
Metastomal filter opening
fraction pumps with filter open
feeding pumps
spitting pumps
UV light:
I
lite-1; mock-ablated
J
lite-1; M1-ablated
K
lite-1; M1/I2-ablated
L
lite-1; M1/I4-ablated
M
lite-1; M1/I2/I4-ablated
N
Pumping inhibition
pumping rate (% feeding rate)
cell ablated: mock M1 M1/I2 M1/I4 M1/I2/I4
lite-1

**Figure 7**

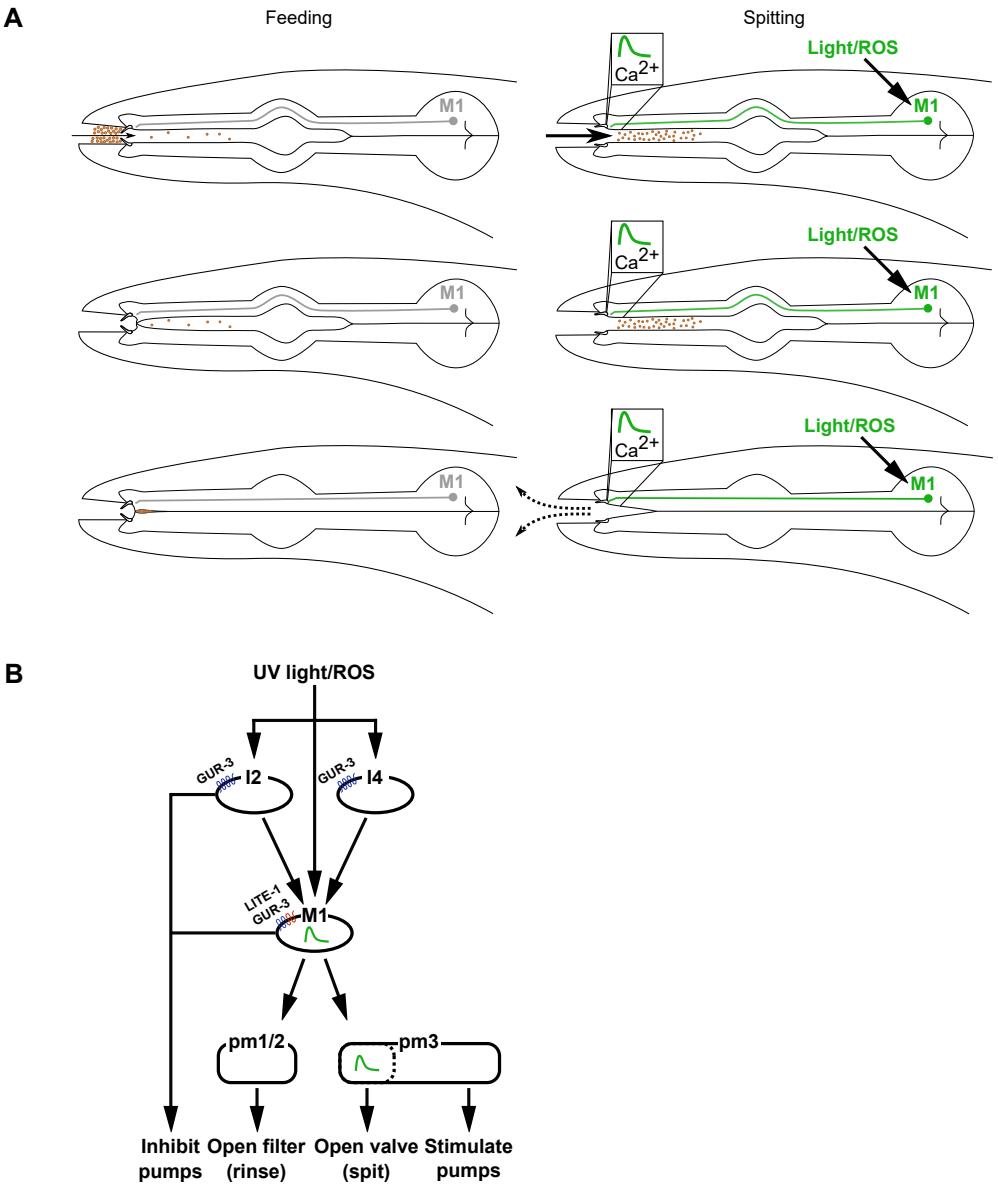
A
Feeding
Spitting
Light/ROS
Ca2+
M1
B
UV light/ROS
GUR-3
I2
I4
LITE-1
pm1/2
pm3
Inhibit pumps
Open filter (rinse)
Open valve (spit)
Stimulate pumps

## Figure 1—figure supplement 1

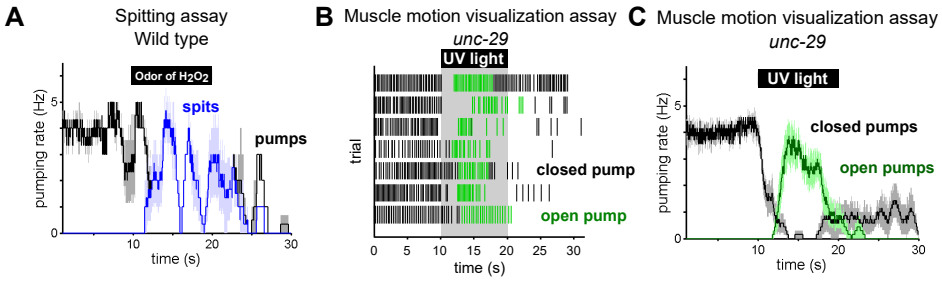

**Figure 2—figure supplement 1**

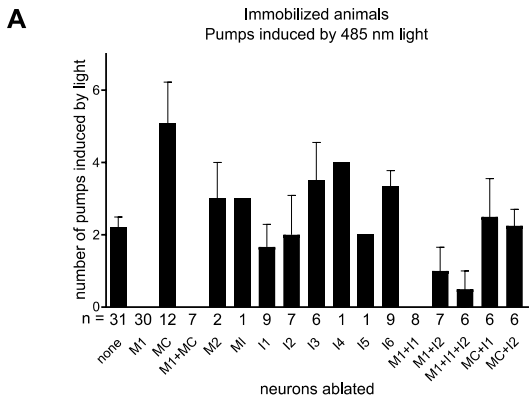


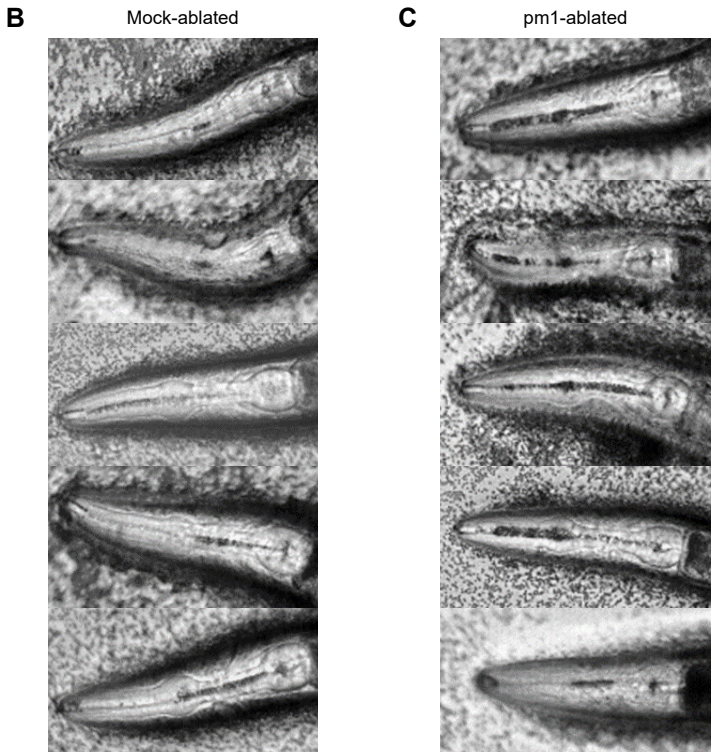

**Figure 3—figure supplement 1**

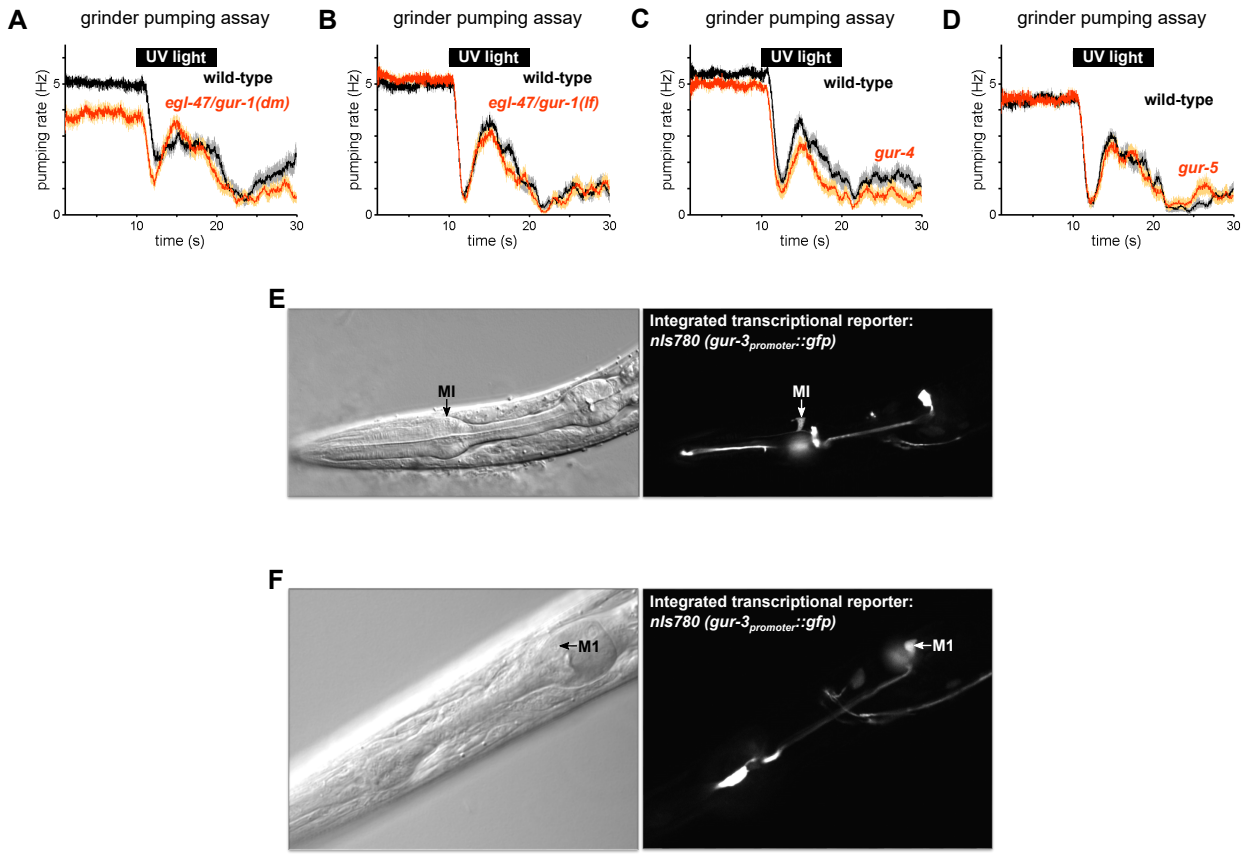

## Figure 4—figure supplement 1

**A** M1 genetic ablation *(nEx2905)*

| Neuron | Percent ablated |
|---|---|
| M1 | 100% (30/30) |
| M2 | 53% (17/32) |

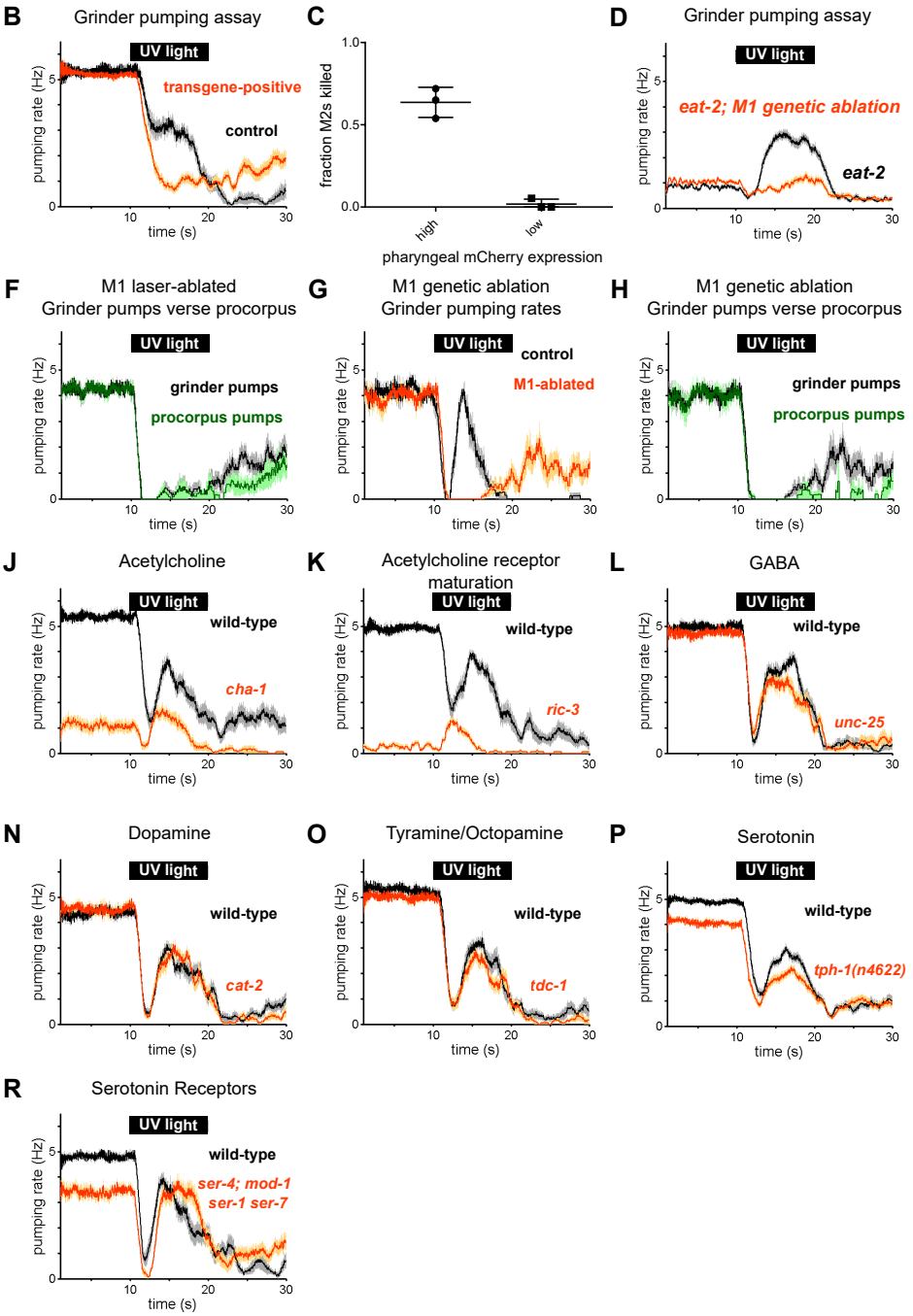

**Figure 4—figure supplement 2, p. 1**

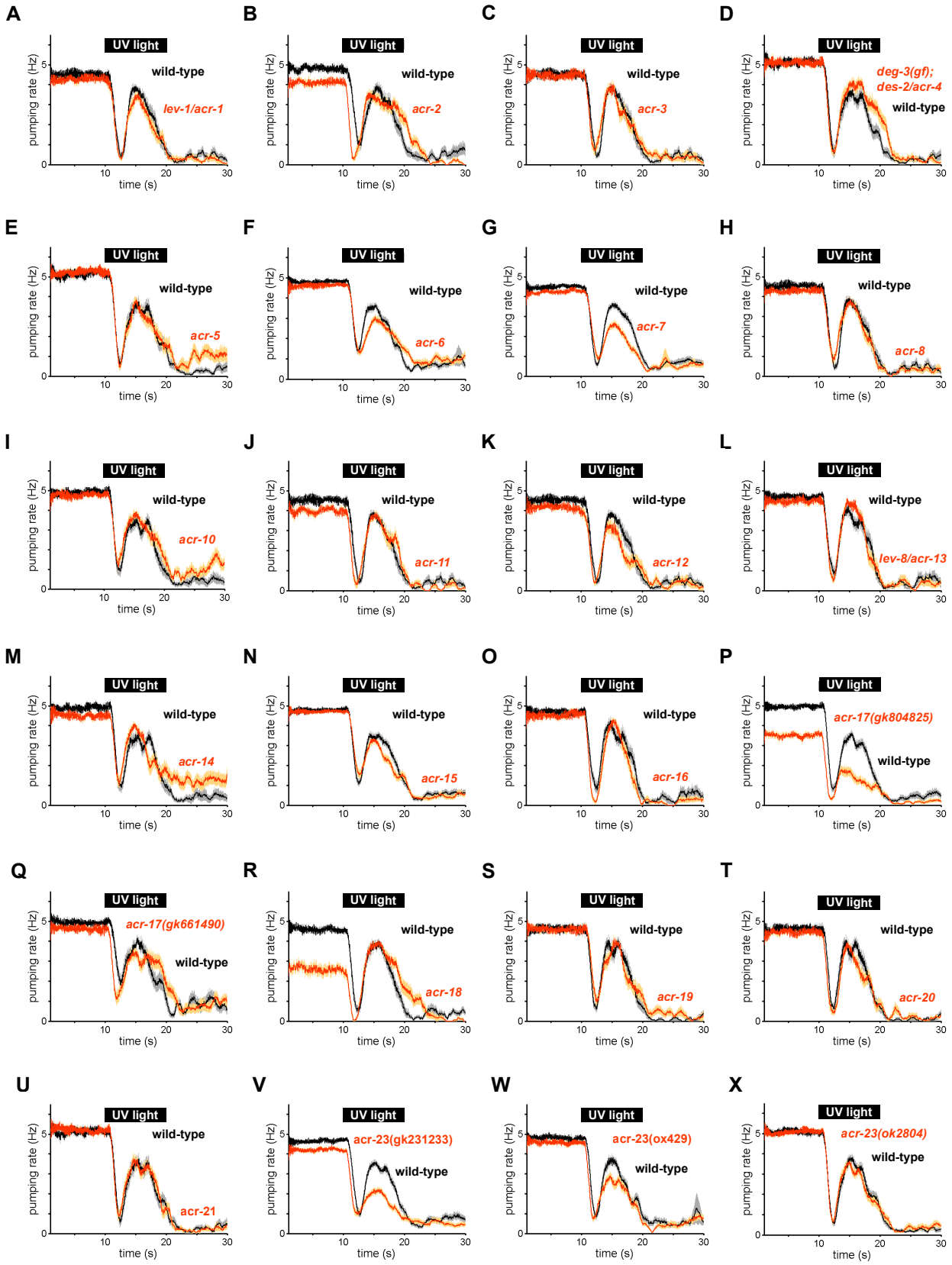
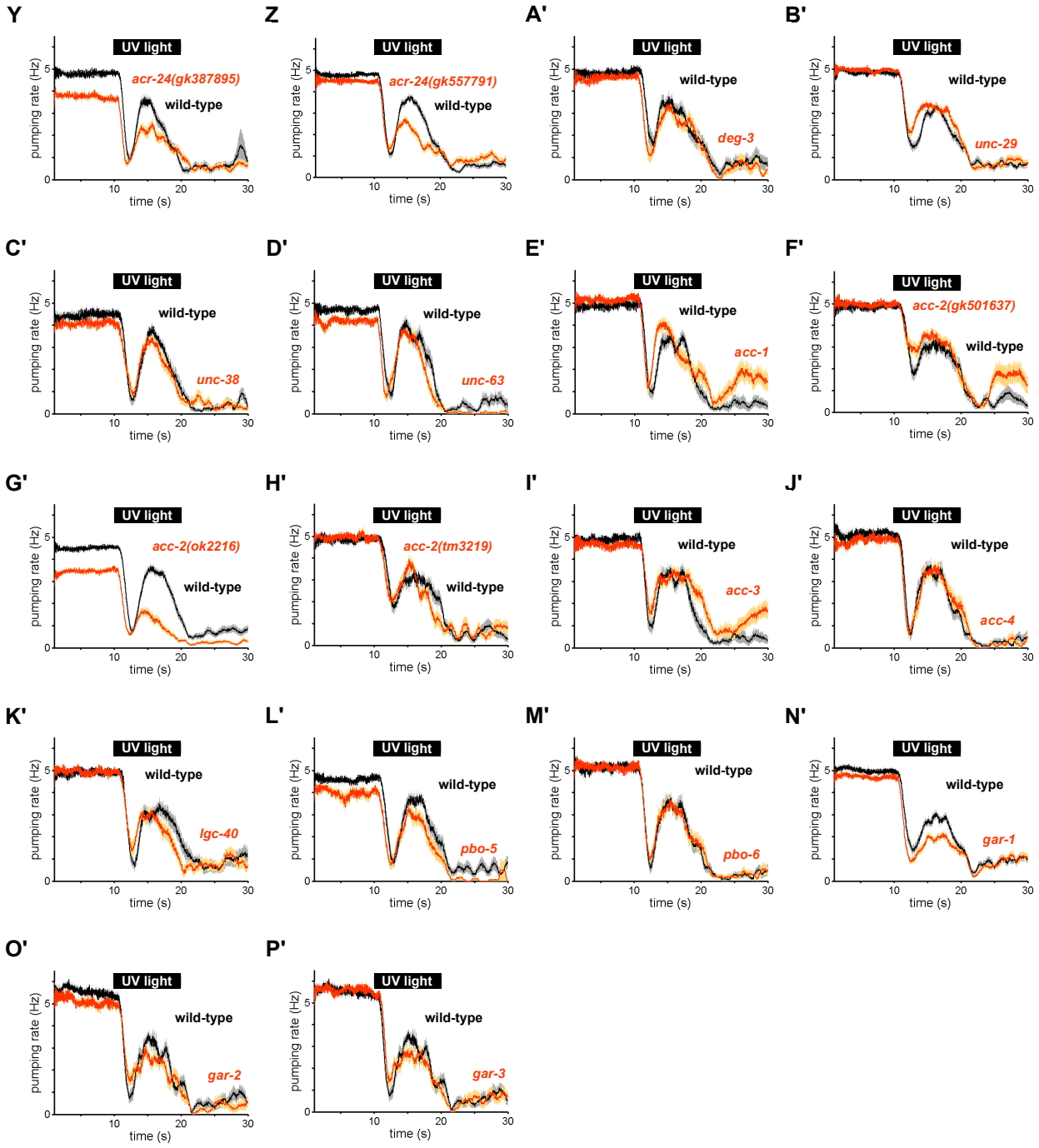
**Figure 4—figure supplement 2, p. 2**